JCI insight

Macrophage-derived PDGF-B induces muscularization in murine and human pulmonary hypertension

Aglaia Ntokou, … , W. Mark Saltzman, Daniel M. Greif

JCI Insight. 2021. https://doi.org/10.1172/jci.insight.139067.

Research In-Press Preview Pulmonology Vascular biology

Graphical abstract

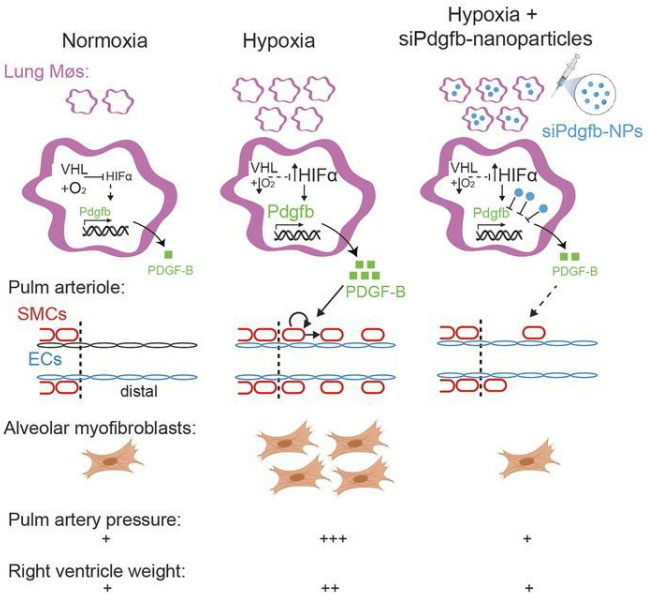

Find the latest version:

https://jci.me/139067/pdf

Macrophage-derived PDGF-B induces muscularization in murine and human pulmonary hypertension

Aglaia Ntokou[1,2], Jui M. Dave[1,2], Amy C. Kauffman[3], Maor Sauler[4], Changwan Ryu[4], John Hwa[1], Erica L. Herzog[4, 5] Inderjit Singh[4], W. Mark Saltzman[3] and Daniel M. Greif [1,2]*

[1]Yale Cardiovascular Research Center, Section of Cardiovascular Medicine and [4]Section of Pulmonary, Critical Care and Sleep Medicine, Department of Internal Medicine and Departments of [2]Genetics, [3]Biomedical Engineering and [5]Pathology
Yale University, New Haven, CT 06511, USA

*To whom correspondence should be addressed:
daniel.greif@yale.edu, 203-737-2040 (phone), 203-737-6118 (FAX)

Conflict of interest: The authors have declared that no conflict of interest exists.

Abstract

Excess macrophages and smooth muscle cells (SMCs) characterize many cardiovascular diseases, but crosstalk between these cell types is poorly defined. Pulmonary hypertension (PH) is a lethal disease in which lung arteriole SMCs proliferate and migrate, coating the normally unmuscularized distal arteriole. We hypothesized that increased macrophage platelet-derived growth factor (PDGF)-B induces pathological SMC burden in PH. Our results indicate that clodronate attenuates hypoxia-induced macrophage accumulation, distal muscularization, PH and right ventricle hypertrophy (RVH). With hypoxia exposure, macrophage Pdgfb mRNA is upregulated in mice, and *LysM-Cre* mice carrying floxed alleles for *hypoxia-inducible factor 1a, 2a* or *Pdgfb* have reduced macrophage Pdgfb and are protected against distal muscularization and PH. Conversely, *LysM-Cre, von-Hippel Lindau*$^{(flox/flox)}$ mice have increased macrophage Hifa and Pdgfb and develop distal muscularization, PH and RVH in normoxia. Similarly, Pdgfb is upregulated in macrophages from human idiopathic or systemic sclerosis-induced pulmonary arterial hypertension patients, and macrophage-conditioned medium from these patients increases SMC proliferation and migration via PDGF-B. Finally, in mice, orotracheal administration of nanoparticles loaded with Pdgfb siRNA specifically reduces lung macrophage Pdgfb and prevents hypoxia-induced distal muscularization, PH and RVH. Thus, macrophage-derived PDGF-B is critical for pathological SMC expansion in PH, and nanoparticle-mediated inhibition of lung macrophage PDGF-B has profound implications as an interventional strategy for PH.

Introduction

Cardiovascular diseases, such as pulmonary hypertension (PH), have a major deleterious impact on human health. Indeed, PH, which is defined by a mean pulmonary arterial pressure greater than 20 mmHg, is responsible for more than 20,000 deaths annually in the United States alone (1, 2). PH is comprised of a heterogenous collection of clinical conditions that are classified into five groups by the World Health Organization (WHO) based on clinical presentation, hemodynamics, pathological findings and therapies (1). Herein, we focus on WHO Group 1 or pulmonary arterial hypertension (PAH), which includes idiopathic (IPAH; formerly classified as primary PH), and Group 3, which is due to lung diseases and/or hypoxia. Approximately one-half of PAH cases are IPAH, heritable or drug-induced, and another important subgroup are associated PAH conditions of which the leading cause is connective tissue disease, predominantly systemic sclerosis (SSc; also known as scleroderma) (3, 4). Unfortunately, PAH is highly morbid and lethal with 50% of patients dying within seven years of initial diagnosis (5). Furthermore, the prognosis of SSc-PAH is dramatically worse than that of IPAH (6). Despite a number of available medications for PAH, no therapies induce reversal or prevent progression of the disease. Similarly, among Group 3 patients, PH portends a substantially worse prognosis for the underlying lung disease (3).

Many cardiovascular diseases, such as atherosclerosis and arterial restenosis, are characterized by excess and aberrant smooth muscle cells (SMCs), and similarly SMC coating of normally unmuscularized distal pulmonary arterioles in PH is a key pathological feature. This hypermuscularization reduces pulmonary arterial compliance which is a strong independent predictor of mortality in IPAH (7). Current treatments for PAH primarily induce vascular dilation, but these therapies do not attenuate the excess muscularization. The treatment gap

largely reflects limits in our understanding of pathogenesis, and hence further investigations into the pathobiology of PH are paramount.

We previously found that specialized pulmonary arteriole SMCs expressing platelet-derived growth factor receptor (PDGFR)-β clonally expand and give rise to pathological distal arteriole SMCs during hypoxia-induced PH, but regulation of this stereotyped process is incompletely understood (8, 9). Upregulation of hypoxia-inducible factor (HIF) 1-α in SMCs plays a key role in distal muscularization, and in addition to such pathways in SMCs themselves, non-cell autonomous regulation is critical (10, 11). In this context, endothelial cells (ECs) are the most highly studied cell type. For instance, the PDGF pathway is integral to vascular SMC development and disease (12, 13), and deletion of the ligand *Pdgfb* in ECs attenuates hypoxia-induced distal pulmonary arteriole muscularization, PH and right ventricle hypertrophy (RVH) (11).

Beyond vascular cell types, immune cells, including monocytes/macrophages, have recently received increasing attention in the context of PH (14, 15). With exposure of mice to hypoxia, monocytes migrate to the lung perivascular space and differentiate into interstitial macrophages (16, 17). Bronchoalveolar lavage of these mice demonstrates an increase in macrophages in the aspirated bronchoalveolar lavage fluid (BALF) as well as in the residual lung (18). Similarly, cells expressing the macrophage marker CD68 are enriched in proximity to vascular obstructive lesions in the lungs of human PAH patients (19). In rodent models of PH, global genetic or pharmacological inhibition of select receptors or agonists expressed by macrophages (e.g., CX3CR1, leukotriene B4) have been shown to mitigate PH (18, 20); however, these products are produced by other cell types as well, raising the issue of macrophage specificity.

Although monocytes/macrophages are undoubtedly important players in the pathogenesis of PH and other vascular diseases, their roles in regulating the biology of SMCs in these contexts are not well established. We recently demonstrated that during the formation of atherosclerotic plaques, clonal expansion of rare SMCs is regulated by bone marrow-derived cells (most likely macrophages) (21). Furthermore, medium conditioned by activated macrophages from atheroprone mice induces aortic SMC migration and proliferation (21, 22). Relevant to PH, hypoxia exposure of macrophages pre-activated by interleukin-4 generates conditioned medium that induces proliferation of pulmonary artery SMCs (PASMCs) (23). In addition, dual inhibition of C-C motif chemokine receptor 2 and 5 attenuates macrophage conditioned medium-induction of PASMC proliferation and migration (24). Finally, we recently found that downregulation of PDGF-B in monocytes/macrophages with the inefficient *Csf1r-Mer-iCre-Mer* modestly inhibits hypoxia-induced pulmonary vascular remodeling, but hemodynamics and underlying pathways were not assessed (11, 25, 26).

Herein, we present findings establishing that lung macrophage-derived PDGF-B plays a key role in pathological SMC expansion and thus, PH and has genuine potential as a therapeutic target. To this end, our studies use mouse models, cell type-specific deletion of multiple genes, human macrophages from IPAH and SSc-PAH patients and *in vivo* nanoparticle-delivered siRNA against Pdgfb. We find that depletion of lung macrophages or *Pdgfb* deletion in myeloid cells attenuates hypoxia-induced distal muscularization, PH and alveolar myofibroblast accumulation. Our results indicate that HIF1-α and HIF2-α are upstream of PDGF-B in macrophages and deletion of either *Hifa* gene in $LysM^{+}$ cells in hypoxia exposed mice has similar effects as *Pdgfb* deletion. As a complementary approach, under normoxic conditions, HIFα gain-of-function in myeloid cells induces lung macrophage accumulation and Pdgfb

expression and distal muscularization, PH and RVH. Medium conditioned by macrophages from IPAH and SSc-PAH patients induce human PASMC (hPASMC) proliferation and migration in a PDGF-B-dependent manner. Finally, our results indicate that orotracheally administered nanoparticles loaded with Pdgfb siRNA markedly attenuates hypoxia-induced lung macrophage Pdgfb expression, distal muscularization, PH, RVH and alveolar myofibroblast accumulation. Taken together, further evaluation of approaches targeting lung macrophage-derived PDGF-B is of high priority as a strategy to combat PH.

Results

Alveolar and parenchymal lung macrophages accumulate in hypoxia and their depletion attenuates distal muscularization and PH

As with our prior studies, immunohistochemical analysis of distal muscularization in the investigations herein focused on specific pulmonary arteriole beds adjacent to identified airway branches left bronchus-first lateral secondary branch-first anterior branch-first lateral or first medial branch (L.L1.A1.L1 or L.L1.A1.M1) (8, 9, 11). Under normoxic conditions, distal arterioles in these beds are unmuscularized but undergo a stereotyped process of muscularization with hypoxia exposure (8, 9, 11).

In addition to developing distal arteriole muscularization and PH, the lungs of mice exposed to hypoxia accumulate excess macrophages (18, 27, 28) (Fig. 1A-C). We initially determined the time course of lung macrophage accumulation during PH in wild type mice maintained in hypoxia (FiO_2 10%) for up to 21 days. The pulmonary vasculature was flushed and then using flow cytometry, we isolated $CD64^{+}Ly6G^{-}$ macrophages from bronchoalveolar lavage fluid (BALF) and from the residual lung after BALF aspiration (Fig. S1). The percent of

macrophages in BALF gradually increases reaching statistical significance on hypoxia day 21 in comparison to normoxia (Fig. 1B). In contrast, macrophages from the residual lung are 2.9±0.5-fold increased by hypoxia day 3 and up to 10.8±1.1-fold increased at hypoxia day 21 (Fig. 1C).

We next evaluated the effects of depletion of alveolar and residual macrophages with clodronate on hypoxia-induced distal muscularization and PH. Liposomes loaded with clodronate or as a control with phosphate buffered saline (PBS) were administered orotracheally to wild type mice at the onset of hypoxia and two times per week during the ensuing 21 days of hypoxia to deplete phagocytes. Mice treated with clodronate have attenuated hypoxia-induced distal muscularization, right ventricular systolic pressure (RVSP; equivalent to pulmonary artery systolic pressure) and RVH as measured by the Fulton index (i.e., weight ratio of the right ventricle [RV] to the sum of the left ventricle [LV] and septum [S]) (Fig. 1D-F). In comparison to control liposomes, treatment with clodronate-loaded liposomes reduces macrophages by ~50% in the BALF and ~65% in the residual lung (Fig. 1G, H). Finally, under basal conditions, the adult lung has very rare myofibroblasts, but we and others have demonstrated that hypoxia induces a marked increase in the number of these cells (8, 29). Herein, we found that depletion of myeloid cells markedly inhibits hypoxia-induced accumulation of alveolar α-smooth muscle actin $(SMA)^+$ myofibroblasts (Fig. I, J).

Lung macrophage Pdgfb is upregulated with hypoxia and *Pdgfb* deletion in the $LysM^+$ or $CSF1R^+$ cells attenuates PH

Exposure of mice to hypoxia increases PDGF-B levels in the whole lung and in lung ECs specifically (9, 11); however, not all lung PDGF-B derives from ECs (9, 11, 30, 31). Thus, we analyzed a time course of Pdgfb expression in $CD64^+Ly6G^-$ macrophages isolated by FACS

from the BALF and residual lung of mice exposed to hypoxia for up to 21 days. Pdgfb mRNA level was measured by qRT-PCR (Table S1) and in comparison to normoxia, is increased within one day of hypoxia and peaks at day 3 at a level of 5.6±0.2 and 9.3±0.2-fold increased for BALF and residual lung, respectively (Fig. 2A, B). Additionally, there is a 2.5±0.4-fold increase in PDGF-B protein in the BALF at hypoxia day 3 compared to normoxia (Fig. S2). To further confirm the upregulation of Pdgfb in monocytes/macrophages, we used LysM-Cre which marks this population (32). *LysM-Cre, ROSA26R$^{(mTmG/mTmG)}$* mice were exposed to hypoxia for 21 days or maintained in normoxia, and then GFP$^+$ cells were isolated by FACS from whole lung. Pdgfb mRNA level is increased by 2.1±0.4 fold in cells isolated from hypoxic mice (Fig. S3A). Similarly, GFP$^+$ cells isolated from BALF of normoxic mice have similarly increased Pdgfb mRNA levels when cultured under hypoxic (3% O_2) as opposed to normoxic conditions (Fig. S3B).

We next evaluated whether monocyte/macrophage-derived Pdgfb contributes to hypoxia-induced PH. Previously, we found that tamoxifen treatment of *Csf1r-Mer-iCre-Mer, Pdgfb$^{(flox/flox)}$* mice modestly attenuates pathological distal pulmonary arteriole muscularization (11), but effects on PH, RVH and myofibroblast accumulation were not studied. Given the inefficiency of this Cre for inducing recombination (25, 26), in the current studies, *Pdgfb$^{(flox/flox)}$* mice carrying *Csf1r-Mer-iCre-Mer* or no Cre were injected with tamoxifen for 15 days (1 mg/day). Mice were then rested for 5 days and subsequently exposed to hypoxia for 21 days. In addition to inhibiting hypoxia-induced distal muscularization, *Pdgfb* deletion in CSF1R$^+$ cells inhibits attenuates RVSP and the Fulton index (Fig. S4). To bypass the inefficiency of the inducible Csf1r-Cre, further studies used the constitutive LysM-Cre to delete *Pdgfb* (Fig. S5A). Importantly, LysM-Cre-mediated *Pdgfb* deletion does not alter Pdgfb levels in lung ECs (Fig. S5B). On the

Pdgfb$^{(flox/flox)}$ background, mice also carrying *LysM-Cre* have attenuated distal muscularization and PH with 21-day hypoxia exposure in comparison to those with no Cre (Fig. 2C, D). When comparing the Fulton index of *LysM-Cre, Pdgfb*$^{(flox/flox)}$ to that of *Pdgfb*$^{(flox/flox)}$ mice, there is a trend toward reduction with hypoxia and increase with normoxia, but these differences do not reach statistical significance (Fig. 2E). However, when the Fulton index differences between hypoxia and normoxia values are stratified by genotype, there is a significant 46±7% reduction in this difference for *LysM-Cre, Pdgfb*$^{(flox/flox)}$ mice (Fig. 2F). Finally, with myeloid cell *Pdgfb* deletion, myofibroblasts are reduced by ~60% at both 3 and 21 days of hypoxia (Figs. 2G, H, S5C, D). Thus, myeloid cell-derived PDGF-B is an important player in hypoxia-induced pulmonary vascular remodeling and PH.

LysM-Cre-mediated deletion of *von-Hippel Lindau* induces Pdgfb expression and pulmonary vascular remodeling in normoxia

Given the critical role of myeloid cell-derived PDGF-B in the pathogenesis of PH, we next endeavored to evaluate mechanisms underlying hypoxia-induced Pdgfb expression by this cell type. Hypoxia-inducible factors (HIFs) are heterodimers of HIF1-β and a HIFα isoform, either HIF1-α or HIF2-α. In mice exposed to hypoxia, EC HIF regulates cell autonomous Pdgfb expression as well as distal muscularization and PH (11, 33, 34). Using oxygen as a substrate, HIFα undergoes proline hydroxylation, a modification that facilitates binding to von-Hippel Lindau (VHL)-E3 ubiquitin ligase and ultimately proteosomal-mediated degradation (35). Thus, HIFα accumulates when oxygen is scare or when the relevant ubiquitination-degradation pathway is inhibited, such as by *Vhl* deletion (11, 36). Under normoxic conditions, in comparison to *Vhl*$^{(flox/flox)}$ mice, *LysM-Cre, Vhl*$^{(flox/flox)}$ mice have reduced Vhl and increased Hif1a, Hif2a and

Pdgfb mRNA levels in BALF cells and increased PDGF-B protein in BALF (Figs. 3A, S6). Furthermore, *Vhl* deletion in myeloid cells induces distal muscularization, PH and RVH in normoxia (Fig. 3B-D) as well as lung macrophage accumulation (Fig. 3E, F).

We then evaluated whether *Vhl* deletion potentiates the effects of a relatively brief (7 day) exposure to hypoxia. At this time point, $Vhl^{(flox/flox)}$ mice carrying *LysM-Cre* have BALF cell Pdgfb mRNA levels that are robustly increased at 7.6±1.2-fold relative to that of mice lacking Cre (Fig. S7A). Furthermore, *Vhl* deletion in $LysM^+$ cells induces markedly enhanced distal muscularization as well as increased RVSP and RVH following brief hypoxia exposure (Fig. S7B-D).

Myeloid cell HIFα regulates Pdgfb expression and hypoxia-induced distal muscularization, RVH and PH

To complement the experiments that delete *Vhl* and thus, induce the HIF pathway, we next pursued studies that delete *Hif1a* or *Hif2a* in $LysM^+$ cells. First, a time course of hypoxia exposure of wild type mice revealed HIF1-α upregulation in BALF cells by hypoxia day 3 (Fig. 4A, B). At this time point, mice on the $Hif1a^{(flox/flox)}$ background and also carrying *LysM-Cre* have reduced levels of Pdgfb and Hif1a in BALF cells in comparison to mice lacking Cre (Figs. 4C, S8A). In addition, accumulation in the lung of cells expressing the macrophage marker CD64 and of myofibroblasts is substantially reduced with *Hif1a* deletion (Fig. 4D-F). Moreover, analysis at hypoxia day 21 revealed that *LysM-Cre,* $Hif1a^{(flox/flox)}$ mice have attenuated distal pulmonary arteriole muscularization, RVSP and Fulton index (Fig. 4G-I). Findings were similar in regard to both hypoxia-induced HIF2-α levels in BALF cells and the effects of *Hif2a* deletion on the lung phenotype of hypoxic *LysM-Cre*, $Hif2a^{(flox/flox)}$ mice (Figs. 5, S8B). Thus, taking

Pdgfb, Vhl, Hif1a and *Hif2a* deletion experiments together, the results suggest that PDGF-B expression by myeloid cells is modulated cell autonomously by both HIFα isoforms and is a key factor regulating pulmonary vascular remodeling and PH.

Macrophage-derived PDGF-B is increased in PAH patients and induces SMC proliferation and migration

Given the prominent role of macrophages and myeloid-derived PDGF-B in pathological lung muscularization in mice, we next sought to extrapolate these findings to human PAH patients (Tables S2, S3). Initially, Pdgfb levels from human macrophages were analyzed. The peripheral blood mononuclear cell (PBMC) fraction was isolated from fresh whole blood of control humans by Ficoll column centrifugation and enriched for monocytes by adherence to plastic (37, 38) (Fig. S9A, B). Adherent cells were incubated with macrophage colony-stimulating factor to differentiate them to macrophages (38), and exposure of macrophages to hypoxia (3% O_2) as opposed to normoxia for 12 h induces a 2.6$\pm$0.6-fold increase in Pdgfb mRNA (Fig. 6A). As strong evidence of the clinical relevance of this work, Pdgfb levels of macrophages differentiated from circulating monocytes of IPAH and SSc-PAH patients are enhanced by 5.1$\pm$1.8 and 10.7$\pm$4.8-fold, respectively, in comparison that of control humans (Fig. 6B, Table S4). Furthermore, PDGF-B protein is increased in medium conditioned by macrophages from these PAH patients compared to controls (Fig. S9C).

We then evaluated the effect of medium conditioned by macrophages from PAH patients on hPASMC proliferation and the role of PDGF-B in this medium. hPASMCs were cultured for 24 h in medium conditioned by newly differentiated macrophages, and BrdU was added for the final 10 h of this incubation. The percent of cells (propidium iodide $[PI]^+$ nuclei) that were

proliferative (i.e., $BrdU^+$) relative to control was determined (Fig. 6C, D, Table S5). For medium conditioned by macrophages derived from IPAH and SSc-PAH patients, there is a relative increase in hPASMC proliferation by 4.6±0.3 and 7.0±1.9-fold, respectively. To evaluate the contribution of PDGF-B to these effects, macrophage conditioned medium was incubated with anti-PDGF-B blocking antibody or IgG control for 1 h prior to adding to hPASMCs. For macrophages derived from control patients, hPASMC proliferation is not changed by anti-PDGF-B pre-treatment whereas this pre-treatment significantly inhibits hPASMC proliferation-induced by medium conditioned by IPAH or SSc-PAH macrophages (Figs. 6E, S9D). A qualitatively similar - albeit less robust - increase in hPASMC proliferation occurs with exposure to medium conditioned by macrophages that were generated from cryopreserved PBMCs of PAH patients (Fig. S9E, Table S6). As with the studies with fresh PBMCs, anti-PDGF-B treatment markedly inhibits hPASMC proliferation in medium conditioned by macrophages from cryopreserved PAH, but not control, PBMCs (Fig. S9F).

Next, a similar approach was used to investigate the effect of medium conditioned by macrophages (from fresh PBMCs) and PDGF-B therein on hPASMC migration. We assessed hPASMC migration from the top of a Boyden chamber towards the bottom chamber containing conditioned medium pre-treated, as in the proliferation studies, with an anti-PDGF-B or IgG control antibody. For IgG control pre-treatment, conditioned medium from IPAH or SSc-PAH macrophages induces migration relative to that from control macrophages by 3.0±0.8 or 4.2±0.8-fold, respectively (Fig. 6F-I, Table S7). Furthermore, in comparison to IgG pre-treatment, anti-PDGF-B pre-treatment reduces hPASMC migration with IPAH or SSc-PAH macrophage conditioned medium by ~40-50%. In contrast, anti-PDGF-B pre-treatment of conditioned medium from control humans does not affect hPASMC migration.

Nanoparticle delivery of siPdgfb attenuates hypoxia-induced PH

After demonstrating the importance of myeloid-derived PDGF-B in experimental PH and the inductive effects of PDGF-B from macrophages of PAH patients on hPASMCs, we next aimed to pharmacologically downregulate this ligand in lung macrophages by delivering nanoparticles formed from a poly(amine-co-ester) [PACE] polymer and Pdgfb siRNA. In prior studies, we have shown that similar nanoparticles are capable for sustained silencing of protein expression in cells that internalize the particles (39). First, 400 or 200 nm diameter nanoparticles composed of acid-ended (poly(pentadecalactone-co-n-methyldiethanolamineco-sebacate) with 50% lactone (PPMS-50COOH) loaded with the dye DiD were orotracheally administered to wild type mice, and 12 h later, flow cytometric analysis was used to evaluate the uptake by lung cells expressing the macrophage marker CD64 (Fig. 7A, B, S10A, B). For both 400 and 200 nm diameter nanoparticles, the vast majority of $CD64^+$ cells are DiD-labeled (>99% in BALF and ~92% in residual lung; Fig. S10C). Similarly, the percent of DiD-labeled cells that are $CD64^+$ is high and equivalent for 400 and 200 nm diameter particles (95$\pm$1% and 93$\pm$3%, respectively) in BALF; however, in the residual lung, these percentages are 86$\pm$1% for 400 nm particles and dropped down to 62$\pm$1% for 200 nm particles (Fig. 7C). To confirm uptake, isolated BALF cells were cultured with DiD-loaded 400 nm nanoparticles for 6 h, and these cells display perinuclear fluorescence (Fig. 7D). Additionally, orotracheal delivery of 400 nm DiD-nanoparticles twice per week for three weeks neither impacts lung mechanics and histology nor leads to uptake by other organs, such as the heart and liver (Figs. S10D-G, S11). Thus, all further experiments were conducted with 400 nm diameter nanoparticles.

We then evaluated whether nanoparticles loaded with siRNA targeting Pdgfb ameliorated the effects of hypoxia exposure on the murine lung. A Pdgfb siRNA oligonucleotide was used that when transfected into BALF cells reduced Pdgfb levels by 91±1% in comparison to Scr RNA treatment (Fig. S12A). Nanoparticles loaded with this siPdgfb or Scr RNA were administered orotracheally at the onset of hypoxia and twice per week for up to 21 days of hypoxia exposure. At hypoxia day 3 or 21, the percent of cells in the whole lung that are $CD64^{+}LysG^{-}$ macrophages does not differ between mice treated with the two nanoparticle types (Figs. 7E-G, S12B-D). We then assayed the effect of siPdgfb-nanoparticles on macrophage Pdgfb RNA levels at day 3, the time of maximal Pdgfb levels (see Fig. 2A, B). Nanoparticles loaded with siPdgfb reduce lung macrophage Pdgfb levels by 86±11% (Fig. 7H). Furthermore, siPdgfb-nanoparticle treatment during 21-day hypoxia exposure markedly attenuates distal pulmonary arteriole muscularization, PH, RVH and accumulation of myofibroblasts (Fig. 7I-M) but does not reverse already well established pulmonary vascular remodeling during chronic hypoxia (Fig. S13). Of note, in the more severe pulmonary vascular disease model of adding weekly Sugen 5416 injections to 21 days of hypoxia, concomitant siPdgfb-nanoparticle treatment leads to modestly reduced distal muscularization, a trend toward slightly lower RVSP that did not reach statistical significance (reduced by 5.2±3.0 mmHg; p=0.18) and a significantly decreased RV weight ratio (Fig. S14).

Discussion

Expansion of the SMC lineage is increasingly recognized as a key factor in diverse cardiovascular diseases (40); however, in these pathological contexts as well as during normal vascular development, our understanding of the non-cell autonomous regulation of SMCs by cell

types beyond ECs is rudimentary. Phagocytes, including macrophages, play fundamental roles in both the innate immune system and the pathogenesis of many cardiovascular pathologies, including PH. During the embryonic period, fetal macrophage precursors are recruited to the normal lung and differentiate into macrophages, and subsequently, these resident macrophages are maintained by local proliferation. In contrast, during PH, increased monocytes are found in the pulmonary vasculature and perivascular regions and give rise to lung macrophages (16, 17). Although vascular SMCs and lung macrophages are undoubtedly important cell types in PH, a critical unresolved issue is whether and how lung macrophages regulate SMCs in this context. Herein, our studies with mouse models of PH and human macrophages from IPAH and SSc-PAH patients demonstrate that macrophage-derived PDGF-B induces pathological SMC expansion and PH and thereby, establish macrophage-derived PDGF-B as a key factor in this paradigm. Moreover, our findings with nanoparticle-derived Pdgfb siRNA demonstrate an intriguing approach to prevent this disease.

Intratracheally administered clodronate-containing liposomes has previously been shown to deplete alveolar macrophages and reduce hypoxia-induced PH and RVH in rats (41). Herein, we demonstrate that such treatment in mice reduces macrophages in the residual lung, which includes interstitial macrophages, and in the BALF (alveolar macrophages) and also attenuates distal muscularization and hemodynamic changes (Fig. 1). Although this approach is beneficial in the short-term, chronically depleting macrophages is not feasible given their integral role in innate immunity. Thus, a preferred strategy is to target specific macrophage-derived gene products.

Along these lines, PDGF is widely implicated in the pathogenesis of PH. In human IPAH, mRNA levels of ligands PDGFA, PDGFB and receptors PDGFRA and PDGFRB are

upregulated in small pulmonary vessels, and PDGFR-β protein is increased in whole lung lysates (42, 43). Mice with a knock-in mutant *Pdgfrb* encoding a protein that is defective in mediating downstream PI3K and PLC-gamma signaling have blunted hypoxia-induced pulmonary vascular remodeling, PH and RVH (43). In a fetal lamb model in which PH is induced by intrauterine partial ligation of the ductus arteriosus, infusion of an anti-PDGF-B aptamer into the pulmonary artery reduces the severity of pulmonary vascular remodeling by one-half and RVH by two-thirds (44). Moreover, global $Pdgfb^{(+/-)}$ mice lack hypoxia-induced distal pulmonary arteriole SMCs whereas EC-specific deletion of *Pdgfb* reduces but does not entirely prevent distal muscularization (9, 11).

Herein, we demonstrate that upon exposing mice to hypoxia, expression of Pdgfb by alveolar and residual lung macrophages is markedly upregulated (by hypoxia day 3), and $Pdgfb^{(flox/flox)}$ mice also carrying *LysM-Cre* or *Csf1r-Mer-iCre-Mer* have substantially attenuated distal muscularization and RVSP (Figs. 2, S2, S4). Additionally, hypoxic *Csf1r-Mer-iCre-Mer,* $Pdgfb^{(flox/flox)}$ mice have a reduced Fulton index. Given that it is constitutive, the LysM-Cre induces more efficient recombination than the inducible Csf1r-Cre; however, LysM-Cre is broadly expressed in myeloid cells (32). Interestingly, in hypoxic *LysM-Cre,* $Pdgfb^{(flox/flox)}$ mice, there is a trend to a reduction in RVH, but it does not reach statistical significance likely because of a trend towards increased Fulton index under normoxia in these mutants. Indeed, the hypoxia-induced increase in RVH stratified by genotype is reduced by ~50% with *Pdgfb* deletion. The explanation for the trend towards enhanced RV weight ratio under basal conditions in *LysM-Cre,* $Pdgfb^{(flox/flox)}$ mice is not clear, but we speculate that myeloid cell-derived PDGF-B may limit RV mass during normal development and/or maintenance.

The aforementioned data indicate that lung macrophage-derived PDGF-B plays an important role in PH; however, the regulation of PDGF-B expression in this cell type is poorly understood. With exposing mice to hypoxia, lung ECs increase Pdgfb levels in a HIF1-α-dependent manner (11), and herein, we found that myeloid cell *Hif1a* or *Hif2a* deletion reduces Pdgfb levels in lung macrophages compared to control mice (Figs. 4, 5). Our data indicate that *Hif1a* deletion in myeloid cells is protective against hypoxia-induced PH, which is in agreement with a recent study (45). In addition, *LysM-Cre, Hif2a*$^{(flox/flox)}$ mice are protected from Schistosoma-induced PH (46), and our results indicate that these mice similarly have attenuated hypoxia-induced PH. Our complementary HIF gain-of-function studies (i.e., myeloid *Vhl* deletion) suggest that lung macrophage HIF is sufficient to induce cell autonomous Pdgfb expression, distal muscularization, PH and RVH under normoxic conditions (Fig. 3). Thus, HIF induces PDGF-B in macrophages, and monocyte/macrophage HIF and PDGF-B are integral to the hypoxic response of the pulmonary vasculature. We suggest that the effects of myeloid cell HIF on pulmonary vascular remodeling and hemodynamics may be largely due to secreted PDGF-B, but other HIF-regulated factors potentially contribute as well.

Our novel findings demonstrate that similar to distal arteriole muscularization, lung macrophages induce accumulation of alveolar myofibroblasts in the hypoxic lung (Fig. 1), and myeloid-derived *Pdgfb*, *Hif1a* and *Hif2a* are critical for this process (Figs. 2, 4, 5). Lung myofibroblasts play a key role in alveolar septal formation during normal alveologenesis in early postnatal mice, and subsequently, in the adult lung, these cells are very rare (8). In fibrotic disease, myofibroblasts are implicated in generating much of the excess extracellular matrix, and macrophages secrete profibrotic factors that recruit and activate myofibroblasts (47). In contrast, the role of monocytes/macrophages in regulating hypoxia-induced alveolar myofibroblasts has

not been previously reported. We recently observed that PDGFR-β^+ cells give rise to over 40% of hypoxia-induced myofibroblasts in the lung (R. Chandran, I. Kabir, A. Sheikh, ELH and DMG, unpublished data) whereas SMA^+ cells are the source of only ~20% (8). These results are in line with other studies suggesting that lung pericytes, which are PDGFR-β^+SMA^-, are an important cell type in PH (8, 48).

Approximately 10-15% of patients with SSc develop PAH, and PAH is the leading cause of mortality in these patients. Indeed, the three year survival is estimated at only 49% for SSc-PAH in comparison to 84% for IPAH patients (6). One factor contributing to this heightened lethality is the muted response to standard anti-PAH treatments in SSc-PAH compared to IPAH patients (49). In addition, anti-PDGFR-β immunohistochemical staining is enhanced in the small vessels of patients with SSc-PAH in comparison to those with IPAH (50). The number of circulating monocytes does not differ between these PAH patient populations (16); however, our results indicate that in macrophages derived from these monocytes, in comparison to control humans, Pdgfb levels are more enhanced in SSc-PAH than in IPAH patients (Fig. 6). Additionally, we found that macrophages from these two classes of PAH patients induce SMC proliferation and migration in a largely PDGF-B-dependent manner. Interestingly, a study published 25 years ago reported that PDGF-B protein level is increased in the BALF of general SSc patients (i.e., patients not evaluated for PH) compared to that of controls (51). Thus, a strategy targeting macrophage-derived PDGF-B may have efficacy in PAH.

Imatinib is a tyrosine kinase inhibitor with activity against BCR-ABL, c-KIT, PDGFR-α and -β with applications in cancers. Daily injections of imatinib reverses pulmonary vascular remodeling, PH and RVH due to monocrotaline in rats or chronic hypoxia in mice (52). Unfortunately, these positive results did not extrapolate to PAH patients in the Imatinib in

Pulmonary Arterial Hypertension, a Randomized Efficacy Study (IMPRES) (53). Overall, 94% of patients discontinued this oral imatinib study, and serious and unexpected adverse effects were common, including subdural hematoma. Notably, however, patients in IMPRES that were able to remain on imatinib for a long duration showed improved functional class and 6 minute walk distance. These results further emphasize the need for anti-PH therapy that targets a specific pathway (e.g., PDGF-B-mediated) in a specific cell type (e.g., macrophages) in the lung.

Herein, we demonstrate that orotracheally administered PPMS polymer-formulated nanoparticles loaded with siRNA targeting Pdgfb substantially downregulate macrophage-derived Pdgfb, preventing hypoxia-induced distal pulmonary arteriole muscularization, PH and RVH (Fig. 7). These nanoparticles are specifically and broadly phagocytosed by lung macrophages. Previous studies have shown that intratracheal or intravenous delivery of nanoparticles carrying agents with efficacy in human PAH, including prostacyclin analogues and sildanefil, attenuates PH in experimental rodent models (54-56). To the best of our knowledge, the only prior report of nanoparticle-mediated RNA interference in this context demonstrated that intravenous delivery of antisense oligonucleotide microRNA (antimiR)-145, which aims to directly target SMCs, mitigates hypoxia/Sugen 5416-induced PH in rats; yet, in addition to the lung, this antimiR accumulates in the liver, spleen and kidney (57). The approach herein of orotracheally administering nanoparticle loaded siRNA is advantageous as it specifically and potently targets a select gene product in lung macrophages and thereby, promises to limit untoward effects. Furthermore, PPMS polymer-formulated nanoparticles are non-toxic and biodegradable and protect their cargo from degradation (58). However, in contrast to the prevention studies, treatment with siPdgfb nanoparticles does not reverse well established pulmonary vascular remodeling and the associated hemodynamic perturbations (Fig. S13).

Future studies should assess whether initiating these nanoparticles in early stages of PH may be beneficial and whether nanoparticles that are smaller and/or specifically engineered for dual targeting of lung ECs (a major PDGF-B source) and macrophages are viable treatments for advanced disease.

A limitation of this study is the predominant use of the murine hypoxia PH model. Indeed, the main cause of death in human PAH is RV failure, and mice exposed to hypoxia develop distal pulmonary arteriole muscularization, PH and RVH without overt RV failure. Yet, a recent echocardiographic study indicates that tricuspid annular plane systolic excursion, a measure of longitudinal RV systolic function that predicts survival in human PAH, is reduced in hypoxic mice (59, 60). Herein, for treatment groups (i.e., clodronate or siPdgfb nanoparticles or LysM-Cre-mediated deletion of *Pdgfb*, *Hif1a* or *Hif2a*), the increase in Fulton index with 21 days of hypoxia (vs. normoxia) was on average 47$\pm$12% of this increase for control groups (i.e., a ~50% reduction). Considering only the 21 day hypoxia groups and not the normoxia groups, treatments (with clodronate or siPdgfb nanoparticles or deletion of *Pdgfb*, *Hif1a* or *Hif2a* with LysM-Cre and/or Csf1r-Mer-iCre-Mer) reduced the Fulton index by an average of ~25%. Importantly, in the combined hypoxia/Sugen 5416 model of severe pulmonary vascular disease, siPdgfb nanoparticles reduce distal muscularization and RVH (Fig. S14).

Taken together, our studies with an experimental model as well as cells isolated form human PAH patients demonstrate that HIFs regulate expression of PDGF-B by lung macrophages and that myeloid cell HIFs and PDGF-B play major roles in SMC remodeling, PH and RVH. Furthermore, nanoparticle-mediated silencing of Pdgfb in lung macrophages is a preventive strategy, and further studies involving nanoparticle-mediated siRNA delivery are warranted to investigate therapies for this devastating disease.

Methods

Animal studies

Mice were obtained from the Jackson Laboratory. C57BL/6 mice were used for wild type studies, and mice carrying *LysM-Cre* (32), *Csf1r-Mer-iCre-Mer* (25), *ROSA26R*$^{(mTmG/mTmG)}$ (61), *Pdgfb*$^{(flox/flox)}$ (62), *Vhl*$^{(flox/flox)}$ (36), *Hif1a*$^{(flox/flox)}$ (63) or *Hif2a*$^{(flox/flox)}$ (64) were previously described. Male and female mice aged 10-16 weeks and sex and age-matched controls were used. For inducible recombination, *Csf1r-Mer-iCre-Mer* mice were injected intraperitoneally with tamoxifen (1 mg/day for 15 days), rested for 5 days and then exposed to hypoxia.

Hypoxia exposure and hemodynamic measurements

Mice were placed for up to 42 days in a hypoxia (10% FiO_2) chamber equipped with a controller and oxygen sensor (BioSpherix). In select mice, Sugen 5416 (S8442, Sigma) was injected subcutaneously (20 mg/kg) on a weekly basis during 21 days of hypoxia. Following hypoxia treatment, RVSP was measured (8). Mice were then euthanized by isoflurane inhalation, and in addition to lung harvesting, hearts were collected to determine the Fulton index, which is the weight ratio of the RV to the sum of the LV and septum (S) (8). The technician conducting hemodynamic measurements was blinded as to treatment group and genotype of mice.

Bronchoalveolar lavage fluid and lung harvesting

Following euthanasia, PBS was perfused through the RV into the lungs. When the whole lung was analyzed, both the right and left lungs were harvested directly after perfusion. For BALF collection, 1 ml PBS was injected through the trachea into alveoli and then aspirated from the trachea. This procedure was repeated once, and the collected BALF was pooled. The BALF

was centrifuged at 830*g* (GS-6R centrifuge, Beckman Coulter) for 10 min at 4°C, and the cell pellet and supernatant were collected and stored at -80°C. For FACS experiments on the residual lung, following BALF removal, the right main stem bronchus was ligated, and the right lung was removed. For immunohistochemistry, the left lung was inflated with 2% low-melt agarose and placed in ice-cold PBS. When the agarose solidified, the left lung was immersed in Dent's fixative (4:1 methanol:DMSO) at 4°C overnight and the next day was washed and stored in 100% methanol at -80°C.

Nanoparticle formulation and administration

Nanoparticles were administered to wild type mice through orotracheal instillation with minor modifications of a previously described approach (65). Briefly, mice were anesthetized by isoflurane inhalation, positioned upright hanging from their teeth with the tongue pulled forward to uncover the top of the trachea. A pipette tip was inserted orotracheally, and a maximum volume of 50 µl was instilled. Clodronate- or Pdgfb siRNA-loaded nanoparticles were administered twice per week starting at the onset of hypoxia and continuing for up 21 days of hypoxia. Mice receiving nanoparticles loaded with the dye DiD were maintained in normoxia for 6 h and then euthanized. For phagocyte depletion, 50 µl of liposomes loaded with 0.25 mg clodronate or PBS and dissolved in PBS (Liposoma Research) were injected.

For nanoparticle uptake assessment or Pdgfb knockdown, PACE nanoparticles composed of acid-ended (poly(pentadecalactone-co-n-methyldiethanolamineco-sebacate) with 50% lactone (PPMS-50COOH) were formulated using a modified single emulsion or double emulsion solvent evaporation technique as previously described (58). Briefly, in formulation of dye-loaded nanoparticles (~200 or ~400 nm in diameter), 0.2 wt% of DiD (ThermoFisher) to polymer was

used. DMSO (10 μL of 10 mg/mL solution) was dissolved into 50 mg of polymer immediately prior to single emulsion formulation. For Pdgfb siRNA and scrambled (Scr) RNA-loaded nanoparticles, the nucleic acid cargo (Dharmacon, 50 nM) was dissolved in sodium acetate buffer (25 mM, pH 5.8) before proceeding to the double emulsion method. Parameters of nanoparticles (stratified by siPdgfb or Scr loading) were assayed, including hydrodynamic diameter (404 ± 8 or 386 ± 7 nm), size distribution (PDI; 0.218 ± 0.004 or 0.238 ± 0.007) and zeta potential (9.4 ± 0.3 or 10.8 ± 0.5 mV) using dynamic light scattering (Zetasizer Pro, Malvern Panalytical) and siRNA loading efficiency (69.6 ± 1.2 or 64.3 ± 0.5%) using QuantIT RiboGreen assay (ThermoFisher). Nanoparticles (0.2 mg) were suspended in 50 μl PBS and administered to mice. To confirm uptake of nanoparticles by macrophages in culture, BALF cell pellet was resuspended in murine cell culture medium (RPMI [Thermo Scientific], 10% fetal bovine serum [FBS; Invitrogen], 5% penicillin/streptomycin [Life Technologies]) and incubated with 0.25 mg/ml DiD-loaded nanoparticles for 6 h at 37°C.

Vibratome section preparation and immunohistochemistry

For immunohistochemical analysis, left lungs stored in 100% methanol were subjected to peroxidase deactivation by incubation in 5% H_2O_2/methanol for 15 min at RT and then sequentially rehydrated in 75%, 50% and 25% and 0% methanol in PBS. A vibratome was used to cut the rehydrated lung into 150 μm thick sections, which were incubated in IHC blocking buffer (5% goat serum in 0.5% Triton X-100/PBS [PBS-T]) at 4°C overnight and then stained with primary antibodies in IHC blocking buffer for 3 days at 4°C. Subsequently, sections were washed three times in PBS-T, incubated in secondary antibodies in IHC blocking buffer overnight at 4°C, washed five times in PBS-T, mounted on slides with Dako mounting medium

and stored at 4°C. Primary antibodies used were rat anti-MECA-32 (1:15, Developmental Studies Hybridoma Bank [DSHB]), rat anti-CD31-FITC clone MEC13.3 (1:250, cat #561813, BD Biosciences), mouse anti-CD64-APC clone X54-5/7.1 (1:250, cat #139306, Biolegend), rat anti-CD68-APC clone FA-11 (1:50, cat #130-102-585, Miltenyi Biotec), rat anti-aquaporin1 (1:100, ab15080, Abcam) and mouse anti-SMA-Cy3 clone 1A4 (1:250, cat #A2547, Sigma). Secondary antibody used was Alexa 488 anti-rat (1:250, cat #A-11006, Invitrogen). Nuclei were stained with DAPI (1:500).

Imaging

Images of the stained sections were acquired using confocal microscopes (PerkinElmer UltraView VOX spinning disc or Leica SP8 point scanning) or an upright microscope (Nikon ECLIPSE 80i). Adobe Photoshop was used to process images. For analysis of distal muscularization, we focused on two specific arteriole beds in the left lung previously described and denoted as L.L1.A1.L1 and L.L1.A1.M1 (8, 9). Their nomenclature derives from the nearest airways that have a stereotyped branching pattern in the adult mouse (8, 66). Based on their diameter and branching pattern, pulmonary arterioles are classified as proximal (P; >75 mm diameter), middle (M; 25 to 75 mm), and distal (D; <25 mm) and the names L, left main bronchus; L1, L2, L3, lateral branches; M1, M2 medial branches; A1, A2 anterior branches (8).

Human studies

All procedures involving human subjects were approved by the Institutional Review Board of Yale University (IRB #1307012431 and #1005006865), and we complied with all

relevant ethical regulations. Written informed consent was obtained from all participants prior to inclusion in the study.

Human monocyte isolation and differentiation to macrophages

Fresh whole blood from IPAH and SSc-PAH patients of the Pulmonary Vascular Disease clinic at Yale University School of Medicine and healthy controls were provided to the Greif lab as de-identified samples. Monocytes were isolated and differentiated into macrophages based on methods described previously (37, 38). In brief, fresh whole blood was diluted 3-fold in HBSS, loaded on a Ficoll-Histopaque column (Fisher Scientific) and centrifuged for 30 min at 830*g*. The peripheral blood mononuclear (PBMC) phase was aspirated, diluted 3-fold in HBSS, centrifuged for 10 min at 830*g*. To ensure platelet removal, the pellet was resuspended in 3 ml HBSS and centrifuged for an additional 10 min at 830*g*. The pellet was then resuspended in RPMI with 10% FBS, and cells were allowed to adhere to a plastic cell culture dish for 1 h at 37°C. Monocytes preferentially adhere to plastic (37) (Fig. S9A, B). Floating cells were discarded, and adherent cells were washed with PBS and either incubated with 5 mM EDTA in PBS for 10 min and collected for staining and flow cytometry or cultured in macrophage differentiation medium (ImmunoCult^{TM}-SF macrophage medium and 1 ng/ml macrophage colony-stimulating factor [both from StemCell Technologies]). The medium was replaced by fresh macrophage differentiation medium on the fourth day. On day 6, the medium was changed to ImmunoCult^{TM}-SF macrophage medium, and 12 h later, conditioned medium was collected, and cells were harvested. For hypoxia studies, macrophages derived from monocytes of healthy donors were exposed to either normoxia or 3% O_2 for 12 h in RPMI supplemented with 1% FBS and 5% penicillin-streptomycin.

hPASMC culture and proliferation assay

hPASMCs (American Type Culture Collection) were cultured up to passage 6 in M199 medium supplemented with 10% FBS, 1% penicillin/streptomycin, 2 ng/ml fibroblast growth factor (Promega), 3 ng/ml epidermal growth factor (Promega). Proliferation was assessed as previously described with minor modifications (67). hPASMCs were trypsinized and cultured overnight on culture slides (BD Falcon) pre-coated with fibronectin (10 μg/mL in PBS). On the next day, the cells were washed with PBS and serum starved overnight in M199 supplemented with 0.5% FBS. Cells were then washed in PBS and cultured for 24 h in medium conditioned by human control or patient-derived macrophages that had or had not been pre-treated with 20 μg/ml IgG control or anti-PDGF-B blocking antibody (R&D Systems) for 1 h at 37°C. For the final 10 h of this incubation, 10 μg/ml BrdU (Sigma) was added to the cells. Slides were fixed in 4% paraformaldehyde for 30 min, rinsed in 0.3% Tris, 1.5% glycine in water for 15 min, incubated in 2N HCl for 30 min at 37°C, washed with 0.1 M boric acid and then incubated in 1% FBS in PBS-T for 1 h. hPASMCs were stained with rat anti-BrdU primary antibody (1:100, BioRad) in 1% FBS in PBS-T for 1 h, washed three times in 0.5% Tween 20 in PBS and then incubated with goat anti-rat secondary antibody conjugated to Alexa 488 (1:500, Molecular Probes) and PI (1:500, Sigma) in 1% FBS in PBS-T for 1 h. Finally, slides were washed three times in 0.5% Tween 20 in PBS and mounted on slides using fluorescence mounting medium (Dako). Proliferation was calculated as the percentage of total PI^+ hPASMCs that were $BrdU^+$. For each control or patient, at least 10 fields of view were scored.

SMC migration assay

Cell migration was assessed in a similar manner as we previously described (67). Briefly, hPASMCs were trypsinized and immediately added to the top of Boyden chamber polycarbonate membranes (Corning Costar, 8 μm pores). The lower compartment of the Boyden chamber contained medium conditioned by human control and patient-derived macrophages that was or was not pre-treated with 20 μg/ml anti-PDGF-B blocking antibody or IgG control for 1 h at 37°C. hPASMCs were allowed to migrate for 8 h towards the lower chamber at which time the membrane was fixed in 4% paraformaldehyde for 30 min, stained with 0.1% Crystal Violet and washed with water. The upper surface of the membrane was scraped with a cotton swab to remove non-migrated cells, and cells on the bottom surface (i.e., migrated cells) were imaged and counted.

Statistics

All data are presented as mean values ± standard deviation. Student's t-test (unpaired, two-tailed) and one-way ANOVA were used to compare means of two groups and multiple groups, respectively (GraphPad Prism software). The statistical significance threshold was set at $p \leq 0.05$. All tests assumed normal distribution.

Study approvals

All procedures involving human subjects were approved by the Institutional Review Board of Yale University (IRB #1307012431 and #1005006865), and we complied with all relevant ethical regulations. Written informed consent was obtained from all participants prior to inclusion in the study. All mouse experiments were approved by the Institutional Animal Care and Use Committee at Yale University.

Author contributions

A.N., J.M.D., A.C.K, M.S., W.M.S. and D.M.G. conceived of and designed experiments and A.N., J.M.D. and A.C.K. performed them. I.S. provided patient samples, C.R. helped with patient clinical data and J.H. and E.L.H. provided infrastructure for the human studies. A.N. and D.M.G. analyzed the results. A.N. and D.M.G prepared the figures and A.N., A.C.K and D.M.G. wrote the manuscript. All authors reviewed and provided input on manuscript.

Acknowledgements

We thank the Greif laboratory, Irinna Papangeli and Georgia Zarkada for scientific input, Timur Yarovinsky and Tarun Tyagi for technical support and Donna Carrano for phlebotomy. ***Funding:*** provided by the NIH (R35HL150766, R01HL125815, R01HL133016, R01HL142674 and R21NS088854 to D.M.G., R01EB00487 to W.M.S., and A.C.K. was supported by a NRSA Postdoctoral Fellowship [T32DK101019]), American Heart Association (Established Investigator Award, 19EIA34660321 to D.M.G.), Department of Army (W81XWH-18-1-0629 to D.M.G.), and March of Dimes (Gene Discovery & Translational Grant, #6-FY15-223 to D.M.G.). ***Competing interests:*** none. ***Data and materials availability:*** all materials reported in this manuscript are commercially available. All the data are available in the main text and supplementary information.

References

1. Simonneau G, Montani D, Celermajer DS, Denton CP, Gatzoulis MA, Krowka M, et al. Haemodynamic definitions and updated clinical classification of pulmonary hypertension. *Eur Respir J.* 2019;53(1).
2. George MG, Schieb LJ, Ayala C, Talwalkar A, and Levant S. Pulmonary hypertension surveillance: United States, 2001 to 2010. *Chest.* 2014;146(2):476-95.
3. Hoeper MM, Humbert M, Souza R, Idrees M, Kawut SM, Sliwa-Hahnle K, et al. A global view of pulmonary hypertension. *Lancet Respir Med.* 2016;4(4):306-22.
4. Galie N, Humbert M, Vachiery JL, Gibbs S, Lang I, Torbicki A, et al. 2015 ESC/ERS Guidelines for the diagnosis and treatment of pulmonary hypertension: The Joint Task Force for the Diagnosis and Treatment of Pulmonary Hypertension of the European Society of Cardiology (ESC) and the European Respiratory Society (ERS): Endorsed by: Association for European Paediatric and Congenital Cardiology (AEPC), International Society for Heart and Lung Transplantation (ISHLT). *Eur Heart J.* 2016;37(1):67-119.
5. Benza RL, Miller DP, Barst RJ, Badesch DB, Frost AE, and McGoon MD. An evaluation of long-term survival from time of diagnosis in pulmonary arterial hypertension from the REVEAL Registry. *Chest.* 2012;142(2):448-56.
6. Fisher MR, Mathai SC, Champion HC, Girgis RE, Housten-Harris T, Hummers L, et al. Clinical differences between idiopathic and scleroderma-related pulmonary hypertension. *Arthritis Rheum.* 2006;54(9):3043-50.
7. Mahapatra S, Nishimura RA, Sorajja P, Cha S, and McGoon MD. Relationship of pulmonary arterial capacitance and mortality in idiopathic pulmonary arterial hypertension. *J Am Coll Cardiol.* 2006;47(4):799-803.

8. Sheikh AQ, Lighthouse JK, and Greif DM. Recapitulation of developing artery muscularization in pulmonary hypertension. *Cell Rep.* 2014;6(5):809-17.

9. Sheikh AQ, Misra A, Rosas IO, Adams RH, and Greif DM. Smooth muscle cell progenitors are primed to muscularize in pulmonary hypertension. *Sci Transl Med.* 2015;7(308):308ra159.

10. Ball MK, Waypa GB, Mungai PT, Nielsen JM, Czech L, Dudley VJ, et al. Regulation of hypoxia-induced pulmonary hypertension by vascular smooth muscle hypoxia-inducible factor-1alpha. *Am J Respir Crit Care Med.* 2014;189(3):314-24.

11. Sheikh AQ, Saddouk FZ, Ntokou A, Mazurek R, and Greif DM. Cell Autonomous and Non-cell Autonomous Regulation of SMC Progenitors in Pulmonary Hypertension. *Cell Rep.* 2018;23(4):1152-65.

12. Andrae J, Gallini R, and Betsholtz C. Role of platelet-derived growth factors in physiology and medicine. *Genes Dev.* 2008;22(10):1276-312.

13. Seidelmann SB, Lighthouse JK, and Greif DM. Development and pathologies of the arterial wall. *Cell Mol Life Sci.* 2014;71(11):1977-99.

14. Florentin J, and Dutta P. Origin and production of inflammatory perivascular macrophages in pulmonary hypertension. *Cytokine.* 2017;100:11-5.

15. Nicolls MR, and Voelkel NF. The Roles of Immunity in the Prevention and Evolution of Pulmonary Arterial Hypertension. *Am J Respir Crit Care Med.* 2017;195(10):1292-9.

16. Florentin J, Coppin E, Vasamsetti SB, Zhao J, Tai YY, Tang Y, et al. Inflammatory Macrophage Expansion in Pulmonary Hypertension Depends upon Mobilization of Blood-Borne Monocytes. *J Immunol.* 2018;200(10):3612-25.

17. Yu YA, Malakhau Y, Yu CA, Phelan SJ, Cumming RI, Kan MJ, et al. Nonclassical Monocytes Sense Hypoxia, Regulate Pulmonary Vascular Remodeling, and Promote Pulmonary Hypertension. *J Immunol.* 2020.

18. Amsellem V, Abid S, Poupel L, Parpaleix A, Rodero M, Gary-Bobo G, et al. Roles for the CX3CL1/CX3CR1 and CCL2/CCR2 Chemokine Systems in Hypoxic Pulmonary Hypertension. *Am J Respir Cell Mol Biol.* 2017;56(5):597-608.

19. Tuder RM, Groves B, Badesch DB, and Voelkel NF. Exuberant endothelial cell growth and elements of inflammation are present in plexiform lesions of pulmonary hypertension. *Am J Pathol.* 1994;144(2):275-85.

20. Tian W, Jiang X, Tamosiuniene R, Sung YK, Qian J, Dhillon G, et al. Blocking macrophage leukotriene b4 prevents endothelial injury and reverses pulmonary hypertension. *Sci Transl Med.* 2013;5(200):200ra117.

21. Misra A, Feng Z, Chandran RR, Kabir I, Rotllan N, Aryal B, et al. Integrin beta3 regulates clonality and fate of smooth muscle-derived atherosclerotic plaque cells. *Nat Commun.* 2018;9(1):2073.

22. Schneider JG, Zhu Y, Coleman T, and Semenkovich CF. Macrophage beta3 integrin suppresses hyperlipidemia-induced inflammation by modulating TNFalpha expression. *Arterioscler Thromb Vasc Biol.* 2007;27(12):2699-706.

23. Vergadi E, Chang MS, Lee C, Liang OD, Liu X, Fernandez-Gonzalez A, et al. Early macrophage recruitment and alternative activation are critical for the later development of hypoxia-induced pulmonary hypertension. *Circulation.* 2011;123(18):1986-95.

24. Abid S, Marcos E, Parpaleix A, Amsellem V, Breau M, Houssaini A, et al. CCR2/CCR5-mediated macrophage-smooth muscle cell crosstalk in pulmonary hypertension. *Eur Respir J.* 2019;54(4).

25. Qian BZ, Li J, Zhang H, Kitamura T, Zhang J, Campion LR, et al. CCL2 recruits inflammatory monocytes to facilitate breast-tumour metastasis. *Nature.* 2011;475(7355):222-5.

26. Epelman S, Lavine KJ, Beaudin AE, Sojka DK, Carrero JA, Calderon B, et al. Embryonic and adult-derived resident cardiac macrophages are maintained through distinct mechanisms at steady state and during inflammation. *Immunity.* 2014;40(1):91-104.

27. Stenmark KR, Fagan KA, and Frid MG. Hypoxia-induced pulmonary vascular remodeling: cellular and molecular mechanisms. *Circ Res.* 2006;99(7):675-91.

28. Rabinovitch M. Pathobiology of pulmonary hypertension. *Annu Rev Pathol.* 2007;2:369-99.

29. Chen YF, Feng JA, Li P, Xing D, Zhang Y, Serra R, et al. Dominant negative mutation of the TGF-beta receptor blocks hypoxia-induced pulmonary vascular remodeling. *J Appl Physiol (1985).* 2006;100(2):564-71.

30. Mornex JF, Martinet Y, Yamauchi K, Bitterman PB, Grotendorst GR, Chytil-Weir A, et al. Spontaneous expression of the c-sis gene and release of a platelet-derived growth factorlike molecule by human alveolar macrophages. *J Clin Invest.* 1986;78(1):61-6.

31. Ross R, Glomset J, Kariya B, and Harker L. A platelet-dependent serum factor that stimulates the proliferation of arterial smooth muscle cells in vitro. *Proc Natl Acad Sci U S A.* 1974;71(4):1207-10.

32. Clausen BE, Burkhardt C, Reith W, Renkawitz R, and Forster I. Conditional gene targeting in macrophages and granulocytes using LysMcre mice. *Transgenic Res.* 1999;8(4):265-77.

33. Cowburn AS, Crosby A, Macias D, Branco C, Colaco RD, Southwood M, et al. HIF2alpha-arginase axis is essential for the development of pulmonary hypertension. *Proc Natl Acad Sci U S A.* 2016;113(31):8801-6.

34. Tang H, Babicheva A, McDermott KM, Gu Y, Ayon RJ, Song S, et al. Endothelial HIF-2alpha contributes to severe pulmonary hypertension due to endothelial-to-mesenchymal transition. *Am J Physiol Lung Cell Mol Physiol.* 2018;314(2):L256-L75.

35. Semenza GL. Hypoxia-inducible factors in physiology and medicine. *Cell.* 2012;148(3):399-408.

36. Haase VH, Glickman JN, Socolovsky M, and Jaenisch R. Vascular tumors in livers with targeted inactivation of the von Hippel-Lindau tumor suppressor. *Proc Natl Acad Sci U S A.* 2001;98(4):1583-8.

37. Bennett WE, and Cohn ZA. The isolation and selected properties of blood monocytes. *J Exp Med.* 1966;123(1):145-60.

38. Karlsson KR, Cowley S, Martinez FO, Shaw M, Minger SL, and James W. Homogeneous monocytes and macrophages from human embryonic stem cells following coculture-free differentiation in M-CSF and IL-3. *Exp Hematol.* 2008;36(9):1167-75.

39. Cui J, Qin L, Zhang J, Abrahimi P, Li H, Li G, et al. Ex vivo pretreatment of human vessels with siRNA nanoparticles provides protein silencing in endothelial cells. *Nature Communications.* 2017;8:191.

40. Mazurek R, Dave JM, Chandran RR, Misra A, Sheikh AQ, and Greif DM. Vascular Cells in Blood Vessel Wall Development and Disease. *Adv Pharmacol.* 2017;78:323-50.

41. Zaloudikova M, Vytasek R, Vajnerova O, Hnilickova O, Vizek M, Hampl V, et al. Depletion of alveolar macrophages attenuates hypoxic pulmonary hypertension but not hypoxia-induced increase in serum concentration of MCP-1. *Physiol Res.* 2016;65(5):763-8.

42. Perros F, Montani D, Dorfmuller P, Durand-Gasselin I, Tcherakian C, Le Pavec J, et al. Platelet-derived growth factor expression and function in idiopathic pulmonary arterial hypertension. *Am J Respir Crit Care Med.* 2008;178(1):81-8.

43. Ten Freyhaus H, Berghausen EM, Janssen W, Leuchs M, Zierden M, Murmann K, et al. Genetic Ablation of PDGF-Dependent Signaling Pathways Abolishes Vascular Remodeling and Experimental Pulmonary Hypertension. *Arterioscler Thromb Vasc Biol.* 2015;35(5):1236-45.

44. Balasubramaniam V, Le Cras TD, Ivy DD, Grover TR, Kinsella JP, and Abman SH. Role of platelet-derived growth factor in vascular remodeling during pulmonary hypertension in the ovine fetus. *Am J Physiol Lung Cell Mol Physiol.* 2003;284(5):L826-33.

45. Kojima H, Tokunou T, Takahara Y, Sunagawa K, Hirooka Y, Ichiki T, et al. Hypoxia-inducible factor-1 alpha deletion in myeloid lineage attenuates hypoxia-induced pulmonary hypertension. *Physiol Rep.* 2019;7(7):e14025.

46. Kumar R, Mickael C, Kassa B, Gebreab L, Robinson JC, Koyanagi DE, et al. TGF-beta activation by bone marrow-derived thrombospondin-1 causes Schistosoma- and hypoxia-induced pulmonary hypertension. *Nat Commun.* 2017;8:15494.

47. Wynn TA, and Barron L. Macrophages: master regulators of inflammation and fibrosis. *Semin Liver Dis.* 2010;30(3):245-57.

48. Yuan K, Liu Y, Zhang Y, Nathan A, Tian W, Yu J, et al. Mural Cell SDF1 Signaling is Associated with the Pathogenesis of Pulmonary Arterial Hypertension. *Am J Respir Cell Mol Biol.* 2020.

49. Girgis RE, Mathai SC, Krishnan JA, Wigley FM, and Hassoun PM. Long-term outcome of bosentan treatment in idiopathic pulmonary arterial hypertension and pulmonary arterial hypertension associated with the scleroderma spectrum of diseases. *J Heart Lung Transplant.* 2005;24(10):1626-31.

50. Overbeek MJ, Boonstra A, Voskuyl AE, Vonk MC, Vonk-Noordegraaf A, van Berkel MP, et al. Platelet-derived growth factor receptor-beta and epidermal growth factor receptor in pulmonary vasculature of systemic sclerosis-associated pulmonary arterial hypertension versus idiopathic pulmonary arterial hypertension and pulmonary veno-occlusive disease: a case-control study. *Arthritis Res Ther.* 2011;13(2):R61.

51. Ludwicka A, Ohba T, Trojanowska M, Yamakage A, Strange C, Smith EA, et al. Elevated levels of platelet derived growth factor and transforming growth factor-beta 1 in bronchoalveolar lavage fluid from patients with scleroderma. *J Rheumatol.* 1995;22(10):1876-83.

52. Schermuly RT, Dony E, Ghofrani HA, Pullamsetti S, Savai R, Roth M, et al. Reversal of experimental pulmonary hypertension by PDGF inhibition. *J Clin Invest.* 2005;115(10):2811-21.

53. Frost AE, Barst RJ, Hoeper MM, Chang HJ, Frantz RP, Fukumoto Y, et al. Long-term safety and efficacy of imatinib in pulmonary arterial hypertension. *J Heart Lung Transplant.* 2015;34(11):1366-75.

54. Ishihara T, Hayashi E, Yamamoto S, Kobayashi C, Tamura Y, Sawazaki R, et al. Encapsulation of beraprost sodium in nanoparticles: analysis of sustained release properties, targeting abilities and pharmacological activities in animal models of pulmonary arterial hypertension. *J Control Release.* 2015;197:97-104.

55. Leifer FG, Konicek DM, Chen KJ, Plaunt AJ, Salvail D, Laurent CE, et al. Inhaled Treprostinil-Prodrug Lipid Nanoparticle Formulations Provide Long-Acting Pulmonary Vasodilation. *Drug Res (Stuttg).* 2018;68(11):605-14.

56. Li B, He W, Ye L, Zhu Y, Tian Y, Chen L, et al. Targeted Delivery of Sildenafil for Inhibiting Pulmonary Vascular Remodeling. *Hypertension.* 2019;73(3):703-11.

57. McLendon JM, Joshi SR, Sparks J, Matar M, Fewell JG, Abe K, et al. Lipid nanoparticle delivery of a microRNA-145 inhibitor improves experimental pulmonary hypertension. *J Control Release.* 2015;210:67-75.

58. Kauffman AC, Piotrowski-Daspit AS, Nakazawa KH, Jiang Y, Datye A, and Saltzman WM. Tunability of Biodegradable Poly(amine- co-ester) Polymers for Customized Nucleic Acid Delivery and Other Biomedical Applications. *Biomacromolecules.* 2018;19(9):3861-73.

59. Zhu Z, Godana D, Li A, Rodriguez B, Gu C, Tang H, et al. Echocardiographic assessment of right ventricular function in experimental pulmonary hypertension. *Pulmonary Circulation.* 2019;9(2):2045894019841987.

60. Forfia PR, Fisher MR, Mathai SC, Housten-Harris T, Hemnes AR, Borlaug BA, et al. Tricuspid annular displacement predicts survival in pulmonary hypertension. *Am J Respir Crit Care Med.* 2006;174(9):1034-41.

61. Muzumdar MD, Tasic B, Miyamichi K, Li L, and Luo L. A global double-fluorescent Cre reporter mouse. *Genesis.* 2007;45(9):593-605.

62. Enge M, Bjarnegard M, Gerhardt H, Gustafsson E, Kalen M, Asker N, et al. Endothelium-specific platelet-derived growth factor-B ablation mimics diabetic retinopathy. *EMBO J.* 2002;21(16):4307-16.

63. Ryan HE, Poloni M, McNulty W, Elson D, Gassmann M, Arbeit JM, et al. Hypoxia-inducible factor-1alpha is a positive factor in solid tumor growth. *Cancer Res.* 2000;60(15):4010-5.

64. Gruber M, Hu CJ, Johnson RS, Brown EJ, Keith B, and Simon MC. Acute postnatal ablation of Hif-2alpha results in anemia. *Proc Natl Acad Sci U S A.* 2007;104(7):2301-6.

65. Ortiz-Muñoz G, and Looney MR. Non-invasive Intratracheal Instillation in Mice. *Bio-protocol.* 2015;5(12):e1504.

66. Metzger RJ, Klein OD, Martin GR, and Krasnow MA. The branching programme of mouse lung development. *Nature.* 2008;453(7196):745-50.

67. Dave JM, Mirabella T, Weatherbee SD, and Greif DM. Pericyte ALK5/TIMP3 Axis Contributes to Endothelial Morphogenesis in the Developing Brain. *Dev Cell.* 2018;44(6):665-78 e6.

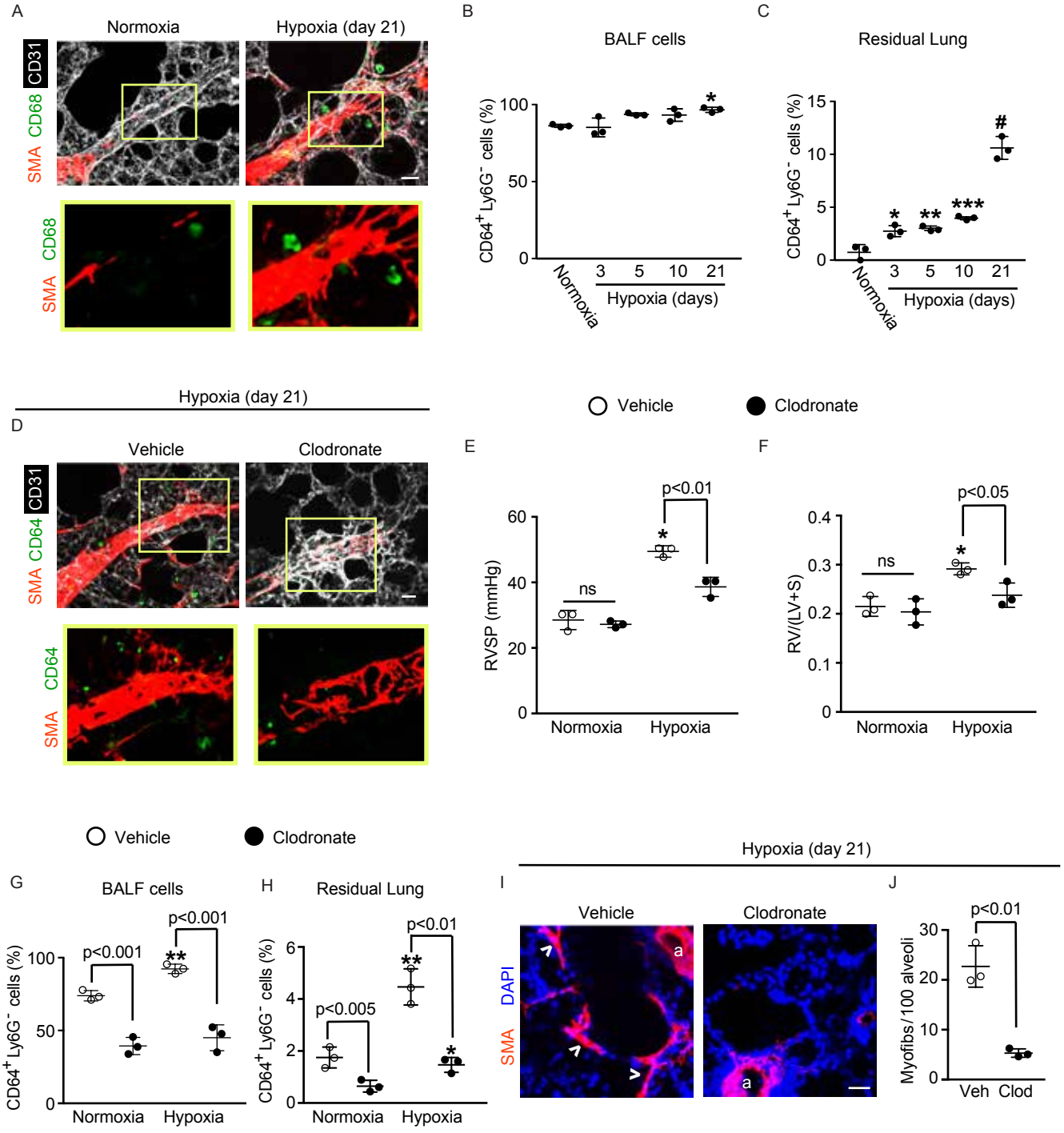
A
Normoxia
Hypoxia (day 21)
CD31
SMA CD68
CD68
SMA
B
BALF cells
CD64+ Ly6G- cells (%)
100
50
0
*
Normoxia
3 5 10 21
Hypoxia (days)
C
Residual Lung
CD64+ Ly6G- cells (%)
15
10
5
0
*
**
***
#
Normoxia
3 5 10 21
Hypoxia (days)
Hypoxia (day 21)
Vehicle
Clodronate
D
Vehicle
Clodronate
CD31
SMA CD64
CD64
SMA
E
RVSP (mmHg)
60
40
20
0
ns
p<0.01
*
Normoxia
Hypoxia
F
RV/(LV+S)
0.4
0.3
0.2
0.1
0
ns
p<0.05
*
Normoxia
Hypoxia
Vehicle
Clodronate
G
BALF cells
CD64+ Ly6G- cells (%)
100
50
0
p<0.001
p<0.001
**
Normoxia
Hypoxia
H
Residual Lung
CD64+ Ly6G- cells (%)
6
4
2
0
p<0.005
p<0.01
**
*
Normoxia
Hypoxia
Hypoxia (day 21)
I
Vehicle
Clodronate
DAPI
SMA
a
a
J
Myofibs/100 alveoli
30
20
10
0
p<0.01
Veh
Clod

Figure 1. Lung macrophages accumulate with hypoxia and are critical for hypoxia-induced pulmonary vascular remodeling and PH. Wild type mice were exposed to hypoxia (10% FiO_2) for up to 21 days or maintained in normoxia as indicated. **A**, Vibratome sections including distal arterioles of the L.L1.A1 regions of left lung were stained for markers of SMCs (α-smooth muscle actin [SMA]), macrophages (CD68) and ECs (CD31). The boxed region is shown as close-ups below. n=6 mice. **B, C**, BALF and residual lung were harvested, and single cell suspensions were subjected to flow cytometric analysis. The percentage of total cells in the given compartment that are $CD64^{+}Ly6G^{-}$ macrophages was determined. n=3 mice per time point. **D-J,** Liposomes containing PBS (vehicle) or clodronate were administered orotracheally at the onset of hypoxia (or normoxia as a control) and two times per week thereafter during the 21-day treatment. In **D,** lung vibratome sections of the L.L1.A1.M1 region were stained for SMA, CD64 and CD31 with boxed regions magnified below. n=4-5 mice. RVSP (**E**) and Fulton index (**F**; weight ratio of the right ventricle [RV] to sum of the left ventricle [LV] and septum [S]) are shown. n=3 mice. In **G, H,** the percent of $CD64^{+}Ly6G^{-}$ macrophages in total cells of the BALF and residual lung was determined. n=3 mice. In **I, J,** alveolar regions were stained for SMA and nuclei (DAPI) and the number of alveolar myofibroblasts (arrowheads) per 100 alveoli was determined. Arterioles are indicated by a. n=3 mice. More than 500 alveoli were quantified per mouse. One-way ANOVA with Tukey's multiple comparison test (*, **, ***, # vs. normoxia, $p < 0.05, < 0.01, < 0.001, < 0.0001$, respectively) was used in **B, C, E-H,** and Student's t-test was used in **J**. ns, not significant. Scale bars, 25 μm.

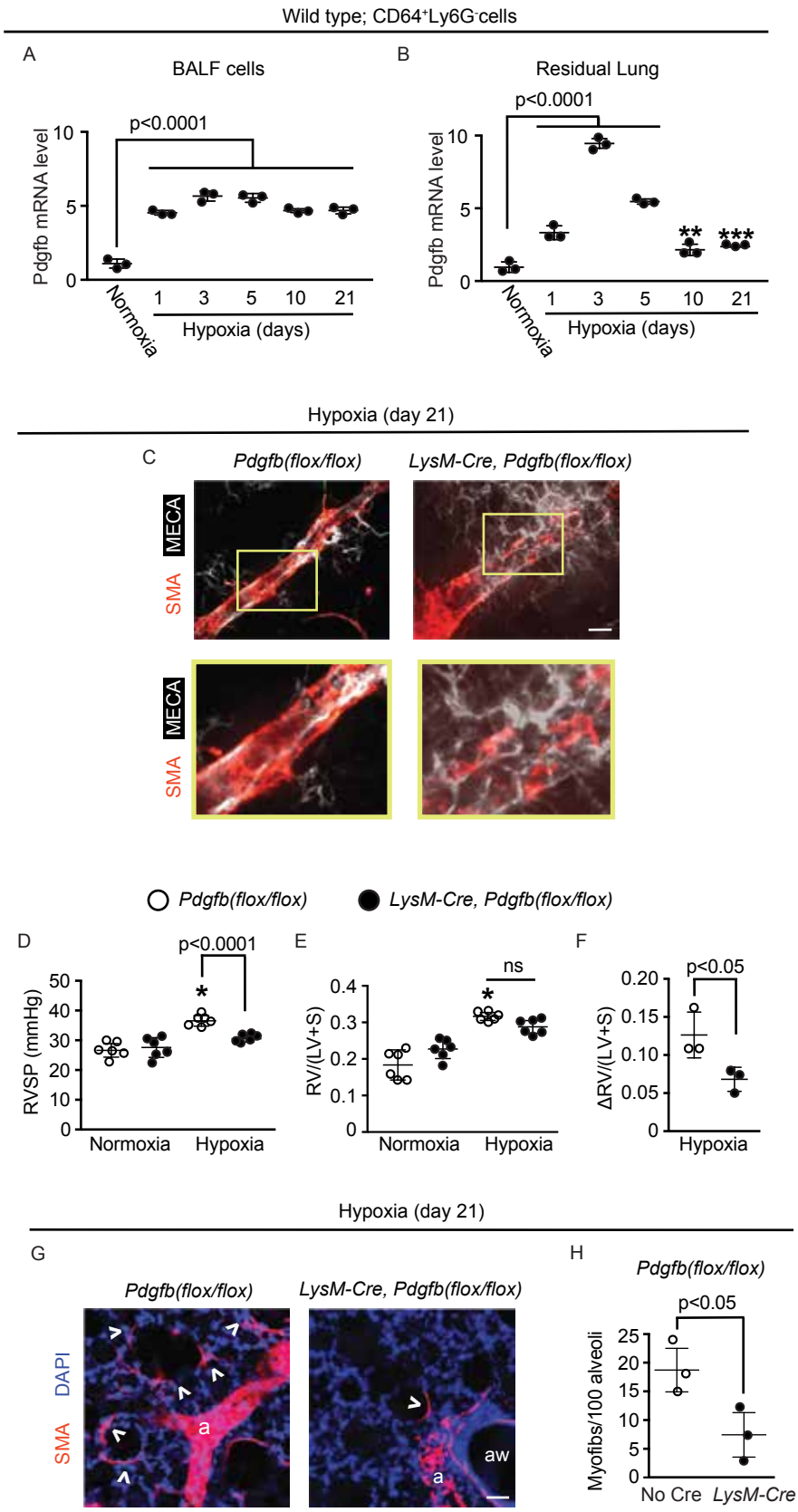
Wild type; CD64+Ly6G- cells
A
BALF cells
p<0.0001
Pdgfb mRNA level
10
5
0
Normoxia
1
3
5
10
21
Hypoxia (days)
B
Residual Lung
p<0.0001
**
***
Hypoxia (day 21)
C
Pdgfb(flox/flox)
LysM-Cre, Pdgfb(flox/flox)
MECA
SMA
Pdgfb(flox/flox)
LysM-Cre, Pdgfb(flox/flox)
D
p<0.0001
RVSP (mmHg)
50
40
30
20
10
0
Normoxia
Hypoxia
E
ns
RV/(LV+S)
0.4
0.3
0.2
0.1
0
F
p<0.05
ΔRV/(LV+S)
0.20
0.15
0.10
0.05
Hypoxia (day 21)
G
Pdgfb(flox/flox)
LysM-Cre, Pdgfb(flox/flox)
DAPI
SMA
a
aw
H
Pdgfb(flox/flox)
p<0.05
Myofibs/100 alveoli
25
20
15
10
5
0
No Cre
LysM-Cre

Figure 2. Lung macrophage Pdgfb levels increase with hypoxia, and *Pdgfb* deletion in LysM$^+$ cells attenuates distal muscularization and PH. A, B, BALF and residual lung CD64$^+$Ly6G$^-$ cells were isolated by FACS from wild type mice exposed to hypoxia (10% FiO_2) for up to 21 days or normoxia as indicated. Pdgfb mRNA levels were measured by qRT-PCR (see Table S1). n=3 mice per time point with qRT-PCR done in triplicate. **C-H,** *Pdgfb*$^{(flox/flox)}$ mice also carrying no Cre or *LysM-Cre* were exposed to hypoxia for 21 days or maintained in normoxia. In **C**, vibratome sections with distal arterioles of the L.L1.A1 lung regions were stained for SMA and EC marker MECA-32. Boxed regions are shown below as close-ups. n=6 mice. RVSP and Fulton index measurements are shown in **D, E**. n=6 mice. In addition, the Fulton index differences between hypoxia and normoxia values stratified by genotype are displayed in **F**. In **G, H,** alveolar regions were stained for SMA and nuclei (DAPI) and the number of alveolar myofibroblasts (arrowheads) per 100 alveoli was determined. Arterioles and airways are indicated by a and aw, respectively. n=3 mice, more than 500 alveoli were quantified per mouse. One-way ANOVA with Tukey's multiple comparison test (*, **, *** vs. normoxia, $p < 0.05, < 0.01, < 0.001$, respectively) was used in **A, B, D, E,** and Student's t-test was used in **F, H.** ns, not significant. Scale bars, 25 μm.

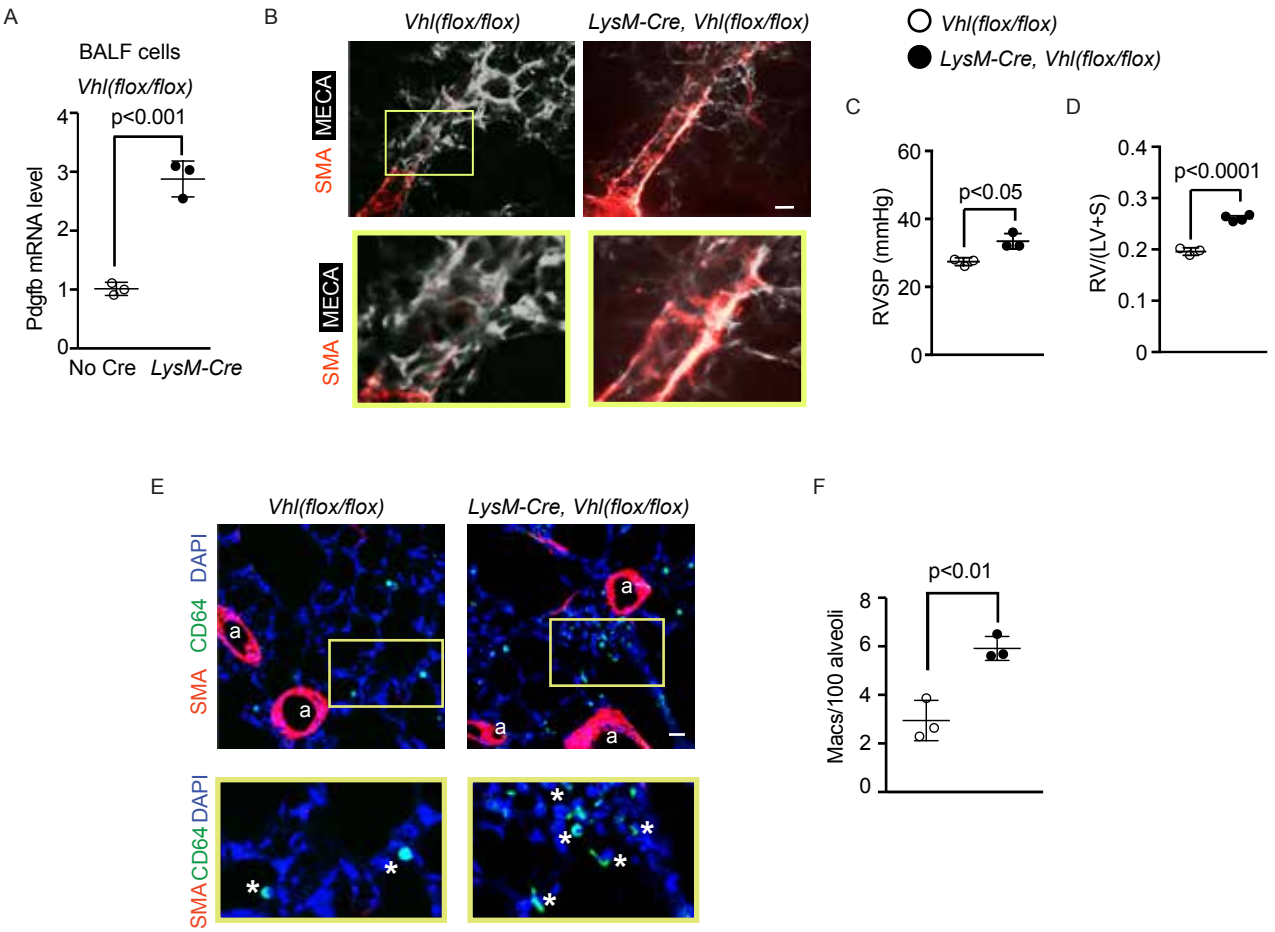
Normoxia (day 49)
A
BALF cells
Vhl(flox/flox)
p<0.001
Pdgfb mRNA level
No Cre
LysM-Cre
B
Vhl(flox/flox)
LysM-Cre, Vhl(flox/flox)
MECA
SMA
C
RVSP (mmHg)
p<0.05
D
RV/(LV+S)
p<0.0001
E
DAPI
CD64
SMA
a
F
Macs/100 alveoli
p<0.01

Figure 3. *Vhl* deletion in LysM^{+} cells induces distal muscularization and PH under normoxia. *Vhl$^{(flox/flox)}$* mice also carrying no Cre or *LysM-Cre* were maintained in normoxia for 49 days after birth. **A,** BALF was isolated and Pdgfb transcript levels were measured by qRT-PCR. **B**, Lung vibratome sections of L.L1.A1.L1 region were stained for SMA and MECA-32 with boxed regions magnified below. RVSP (**C**) and Fulton index (**D**) are shown. **E,** Lung vibratome sections were stained for SMA, CD64 and nuclei (DAPI) with arterioles labeled with a. Boxed regions shown are shown below as close-ups, and the number of macrophages (asterisks) quantified per 100 alveoli in (**F**). More than 500 alveoli per mouse were quantified. n=3 mice. Student's t-test was used in **A, C, D, F.** Scale bars, 25 μm.

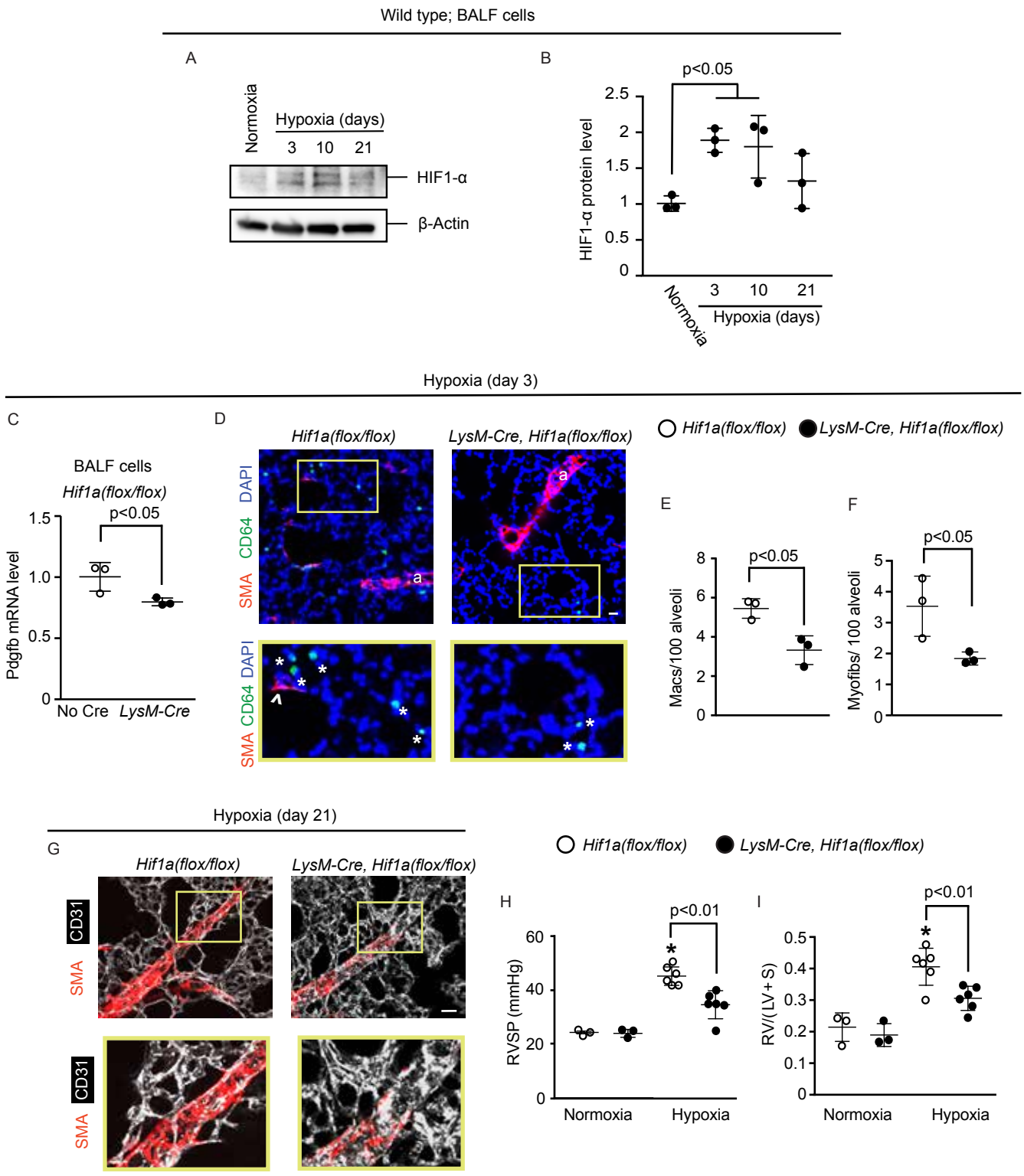
Wild type; BALF cells
A
Normoxia
Hypoxia (days)
3 10 21
HIF1-α
β-Actin
B
p<0.05
HIF1-α protein level
2.5
2
1.5
1
0.5
0
Normoxia
3 10 21
Hypoxia (days)
Hypoxia (day 3)
C
BALF cells
Hif1a(flox/flox)
p<0.05
Pdgfb mRNA level
1.5
1.0
0.5
0
No Cre LysM-Cre
D
Hif1a(flox/flox)
LysM-Cre, Hif1a(flox/flox)
DAPI
CD64
SMA
a
Hif1a(flox/flox)
LysM-Cre, Hif1a(flox/flox)
E
p<0.05
Macs/100 alveoli
8
6
4
2
0
F
p<0.05
Myofibs/ 100 alveoli
5
4
3
2
1
0
Hypoxia (day 21)
G
Hif1a(flox/flox)
LysM-Cre, Hif1a(flox/flox)
CD31
SMA
Hif1a(flox/flox)
LysM-Cre, Hif1a(flox/flox)
H
p<0.01
RVSP (mmHg)
60
40
20
0
Normoxia
Hypoxia
I
p<0.01
RV/(LV+S)
0.5
0.4
0.3
0.2
0.1
0
Normoxia
Hypoxia

Figure 4. *Hif1a* deletion in myeloid cells attenuates hypoxia-induced Pdgfb expression, distal muscularization and PH. A, B, BALF cells were isolated from normoxic or hypoxic (10% FiO_2, up to 21 days) wild type mice. HIF1-α and β-actin protein were assessed by Western blot (**A**) with densitometry of HIF1-α relative to β-actin (**B**). n=3 mice per time point. **C-I,** *Hif1a*$^{(flox/flox)}$ mice also carrying no Cre or *LysM-Cre* were exposed to hypoxia for 3 or 21 days. At hypoxia day 3, Pdgfb transcript levels of BALF cells were determined by qRT-PCR (**C**). Lung vibratome sections were stained for SMA, macrophage marker CD64 and nuclei (DAPI) with the boxed regions shown as close-ups below (**D**). The number of macrophages (asterisks) and alveolar myofibroblasts (arrowheads) were quantified per 100 alveoli (**D-F**). n=3-5 mice, qRT-PCR was done in triplicate. More than 700 alveoli were quantified per mouse. At hypoxia day 21, vibratome sections with distal arterioles in the L.L1.A1.L1 area were stained for SMA and CD31 (**G**), and RVSP and the Fulton index were measured as shown in **H, I**. n=3 mice. One-way ANOVA with Tukey's multiple comparison test was used in **B, H, I** (* vs. normoxia, $p < 0.05$), and Student's t-test was used in **C, E, F.** Scale bars, 25 μm.

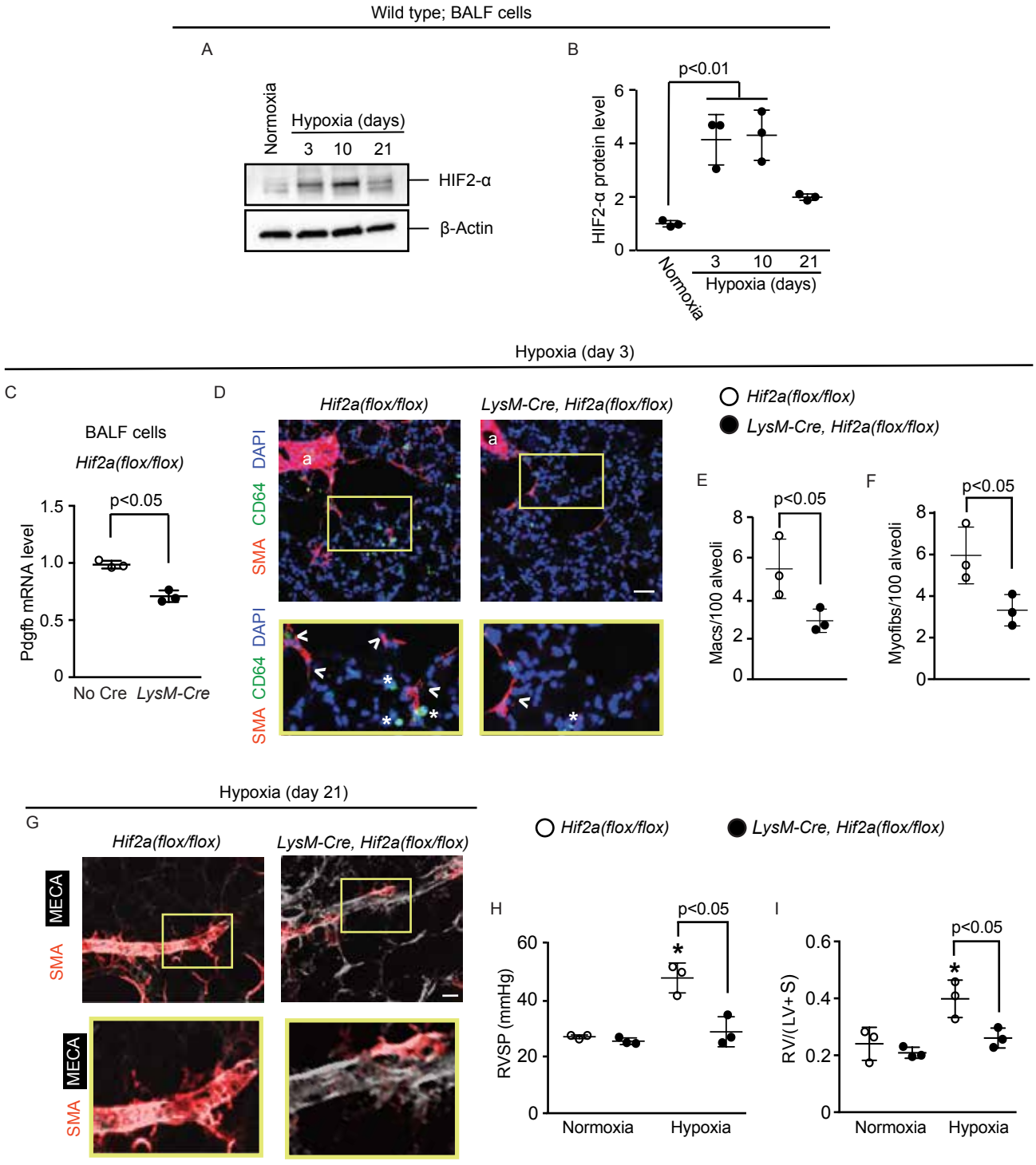
Wild type; BALF cells
A
Normoxia
Hypoxia (days)
3 10 21
HIF2-α
β-Actin
B
p<0.01
HIF2-α protein level
Normoxia
3 10 21
Hypoxia (days)
Hypoxia (day 3)
C
BALF cells
Hif2a(flox/flox)
p<0.05
Pdgfb mRNA level
No Cre LysM-Cre
D
Hif2a(flox/flox)
LysM-Cre, Hif2a(flox/flox)
DAPI
CD64
SMA
E
p<0.05
Macs/100 alveoli
F
p<0.05
Myofibs/100 alveoli
Hypoxia (day 21)
G
Hif2a(flox/flox)
LysM-Cre, Hif2a(flox/flox)
MECA
SMA
H
p<0.05
RVSP (mmHg)
Normoxia
Hypoxia
I
p<0.05
RV/(LV+S)
Normoxia
Hypoxia

Figure 5. Deletion of *Hif2a* in LysM^{+} cells attenuates hypoxia-induced Pdgfb expression, distal muscularization and PH. A, B, BALF cells were isolated from wild type mice exposed to normoxia or hypoxia (10% FiO_2) for up to 21 days. Western blot was used to assess HIF2-α and β-actin protein levels (**A**) with densitometry of HIF2-α relative to β-actin (**B**). n=3 mice per time point. **C-I,** *Hif2a$^{(flox/flox)}$* mice also carrying no Cre or *LysM-Cre* were exposed to hypoxia for 3 or 21 days. At hypoxia day 3, BALF cells were isolated with Pdgfb mRNA levels determined by qRT-PCR (**C**), and vibratome sections of the lung were stained for SMA, CD64 and nuclei (DAPI) with close-ups of the boxed regions shown below (**D**). The number of macrophages (asterisks) and alveolar myofibroblasts (arrowheads) were quantified per 100 alveoli (**D-F**). n=3-5 mice, qRT-PCR was done in triplicate. More than 700 alveoli were quantified per mouse. At hypoxia day 21, vibratome sections with distal arterioles in the L.L1.A1.L1 area were stained for SMA and MECA-32 (**G**), and RVSP and the Fulton index were measured (**H, I**). n=3 mice. One-way ANOVA with Tukey's multiple comparison test was used in **B, H, I** (* vs. normoxia, $p < 0.05$), and Student's t-test was used in **C, E, F.** Scale bars, 50 μm (**D**) and 25 μm (**G**).

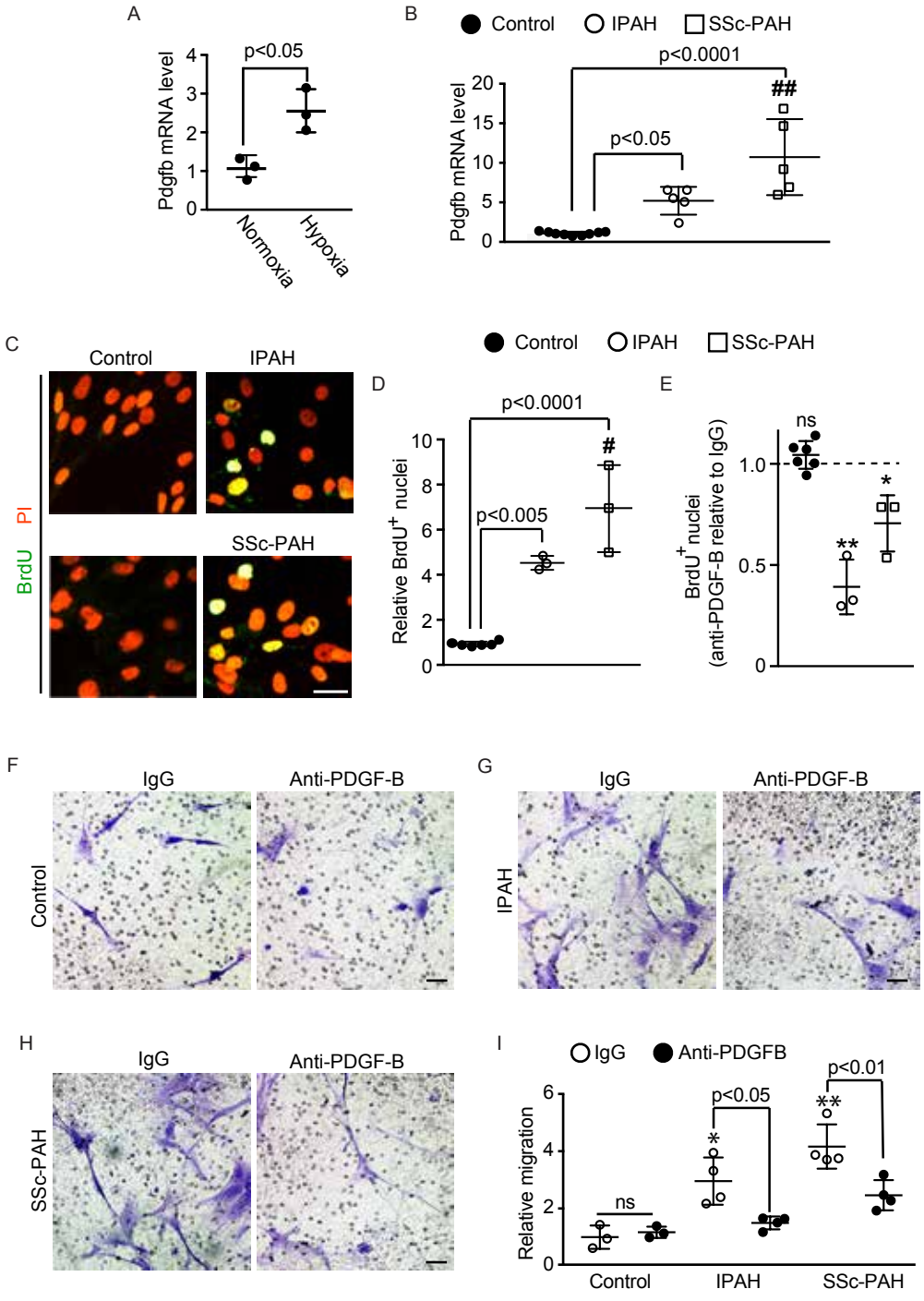
A
Pdgfb mRNA level
p<0.05
Normoxia
Hypoxia
B
Control
IPAH
SSc-PAH
Pdgfb mRNA level
p<0.0001
p<0.05
##
C
Control
IPAH
SSc-PAH
BrdU
PI
D
Control
IPAH
SSc-PAH
Relative BrdU+ nuclei
p<0.0001
p<0.005
#
E
BrdU+ nuclei (anti-PDGF-B relative to IgG)
ns
**
*
F
IgG
Anti-PDGF-B
Control
G
IgG
Anti-PDGF-B
IPAH
H
IgG
Anti-PDGF-B
SSc-PAH
I
IgG
Anti-PDGFB
Relative migration
p<0.05
p<0.01
ns
*
**
Control
IPAH
SSc-PAH

Figure 6. PDGF-B secreted by macrophages from PAH patients promotes hPASMC proliferation and migration. Monocytes were isolated from peripheral blood mononuclear cells of human controls and IPAH or SSc-PAH patients and differentiated into macrophages in culture. **A,** Macrophages derived from human control monocytes were cultured under normoxic or hypoxic (3% O_2) conditions for 12 h, and then Pdgfb mRNA levels were measured by qRT-PCR. n=3 humans (two females and one male, aged 30-60 years old) with qRT-PCR done in triplicate. **B,** qRT-PCR was used to assay Pdgfb mRNA levels of macrophages from controls and PAH patients. n=5 humans per PAH diagnostic class and n=9 controls (see Table S4) with qRT-PCR done in triplicate. **C-E,** hPASMCs were cultured for 24 h with medium preconditioned by control and patient macrophages. BrdU was included in the last 10 h of this incubation. Cells were then stained for BrdU and nuclei (propidium iodide [PI]). In **D**, the percent of total cells (PI^+ nuclei) expressing BrdU for control humans and patients was normalized to this percentage for controls. In **E,** anti-PDGF-B blocking antibody or control IgG was added to the conditioned medium 1 h prior to incubation with hPASMCs. Results are the ratio of the percent of total (PI^+) cells that are $BrdU^+$ for anti-PDGF-B treatment relative to IgG treatment, stratified by patient diagnostic class. n=3 humans per PAH diagnostic class and n=6 controls (see Table S5), 10 microscopic fields per human, 30-60 cells per field. **F-I,** Medium preconditioned by control or patient macrophages was treated with anti-PDGF-B blocking or control IgG antibody for 1 h and then placed in the bottom chamber of a Boyden apparatus. hPASMCs were added to the top chamber to assess migration toward the conditioned medium for 8 h. Migrated cells (i.e., on the membrane's bottom surface) were stained with Crystal Violet. In **I,** quantification of the migrated cells relative to control patients, IgG treatment is shown. n=4 humans per PAH class and n=3 controls (see Table S7), 5 microscopic fields per human, 8-90 cells per field. One-way ANOVA

with Tukey's multiple comparison test (**B, D, I**) and Student's t-test were used (**A, E**). #, ## vs. IPAH, $p<0.05$, <0.01, and *, **, ns vs. corresponding IgG controls, $p<0.05$, <0.01, not significant, respectively. Scale bars, 25 μm (**C**) and 50 μm (**F-H**).

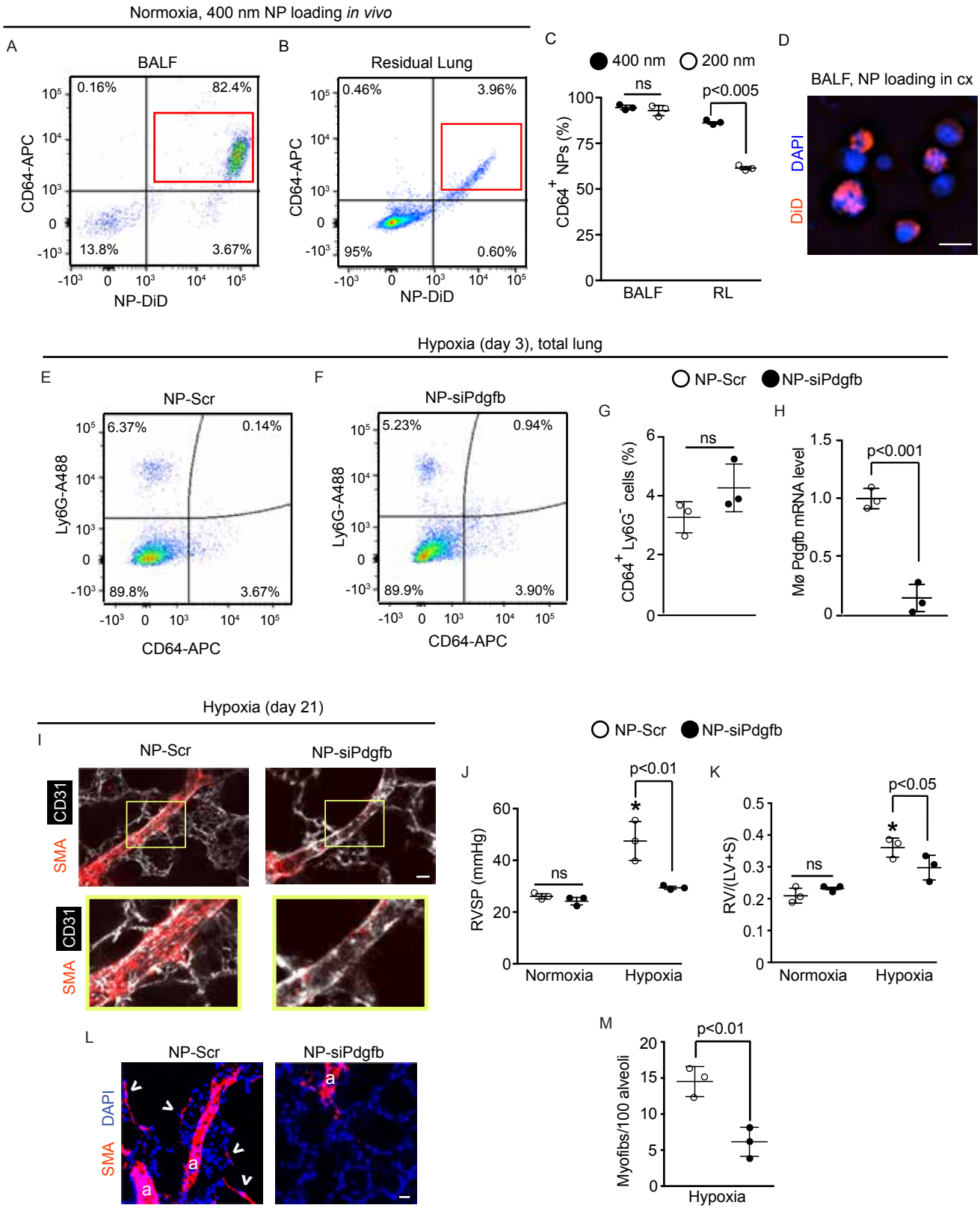
Normoxia, 400 nm NP loading *in vivo*
A
BALF
0.16%
82.4%
13.8%
3.67%
CD64-APC
NP-DiD
B
Residual Lung
0.46%
3.96%
95%
0.60%
C
400 nm
200 nm
ns
p<0.005
CD64+ NPs (%)
BALF
RL
D
BALF, NP loading in cx
DAPI
DiD
Hypoxia (day 3), total lung
E
NP-Scr
6.37%
0.14%
89.8%
3.67%
Ly6G-A488
CD64-APC
F
NP-siPdgfb
5.23%
0.94%
89.9%
3.90%
NP-Scr
NP-siPdgfb
G
ns
CD64+ Ly6G- cells (%)
H
p<0.001
Mø Pdgfb mRNA level
Hypoxia (day 21)
I
NP-Scr
NP-siPdgfb
CD31
SMA
J
p<0.01
ns
RVSP (mmHg)
Normoxia
Hypoxia
K
p<0.05
ns
RV/(LV+S)
L
NP-Scr
NP-siPdgfb
DAPI
SMA
a
M
p<0.01
Myofibs/100 alveoli
Hypoxia

Figure 7. Nanoparticle-mediated knockdown of Pdgfb attenuates distal arteriole muscularization, myofibroblast accumulation and PH. A, B, Nanoparticles (diameter 400 nm) loaded with the dye DiD were administered orotracheally to normoxic mice, and 12 h later, cells from BALF and residual lung were stained for CD64 and subjected to flow cytometric analysis. **C**, Quantification of experiments represented in **A, B** and Figure S10A, B showing the percentage of BALF or residual lung (RL) cells containing DiD^+ nanoparticles (diameter 400 or 200 nm as indicated) that express CD64. n=3 mice per treatment. **D,** BALF cells were harvested from normoxic mice, cultured with DiD-loaded 400 nm nanoparticles for 6 h and then stained for nuclei (DAPI). **E-M**, Nanoparticles of 400 nm diameter were loaded with siRNA targeted against Pdgfb or scrambled (Scr) RNA and then administered to mice at the onset of hypoxia and twice per week thereafter. In **E, F,** lungs were isolated from mice at hypoxia day 3, stained for Ly6G and CD64 and subjected to flow cytometry, and the percent of $CD64^+Ly6G^-$ macrophages was quantified in **G**. n=3 mice per treatment. In **H,** Pdgfb RNA levels of $CD64^+Ly6G^-$ macrophages isolated as in **E, F** were quantified by qRT-PCR. n=3 mice per treatment with qRT-PCR done in triplicate. In **I-M,** mice were treated with hypoxia for 21 days or maintained in normoxia. For hypoxic mice, sections containing distal arterioles in the L.L1.A1 area (**I**) or alveolar region (**L**) were stained for CD31 and SMA. Boxed regions are shown below as close-ups. RVSP (**J**), Fulton index (**K**) and number of myofibroblasts (arrowheads) per 100 alveoli were measured. More than 500 alveoli per mouse were quantified. Arterioles are labeled with a in **L**. n=3 mice per treatment group. One-way ANOVA with Tukey's multiple comparison test (**C, J, K**) and Student's t-test were used (**G, H, M**). * vs. normoxia, $p<0.05$. ns, not significant. Scale bars, 10 μm (**D**) and 25 μm (**I, L**).